

LEHIGH UNIVERSITY

INSTITUTE OF
FRACTURE AND SOLID
MECHANICS

NORMAL AND RADIAL IMPACT OF COMPOSITES WITH EMBEDDED PENNY-SHAPED CRACKS

BY

G. C. SIH AND E. P. CHEN

FEBRUARY 1979

MATERIALS AND STRUCTURES DIVISION

NASA-LEWIS RESEARCH CENTER

CLEVELAND, OHIO 44135

DISTRIBUTION STATEMENT A

Approved for public release;
Distribution Unlimited

DTIC QUALITY INSPECTED 1

19960229 111

PLASTIC
33184

1. Report No. NASA CR 159538	2. Government Accession No.	3. Recipient's Catalog No.	
4. Title and Subtitle NORMAL AND RADIAL IMPACT OF COMPOSITES WITH EMBEDDED PENNY-SHAPED CRACKS		5. Report Date February 1979	6. Performing Organization Code
7. Author(s) Dr. G. C. Sih and Dr. E. P. Chen		8. Performing Organization Report No.	
9. Performing Organization Name and Address Lehigh University Institute of Fracture and Solid Mechanics Bethlehem, PA 18015		10. Work Unit No.	
12. Sponsoring Agency Name and Address National Aeronautics and Space Administration Washington DC 20546		11. Contract or Grant No. NSG 3179	
		13. Type of Report and Period Covered Interim Report	
		14. Sponsoring Agency Code	
15. Supplementary Notes Project Manager: Christos C. Chamis Materials and Structures Division NASA-Lewis Research Center 21000 Brookpark Road, M.S. 49-3 Cleveland, OH 44135			
16. Abstract A method is developed for the dynamic stress analysis of a layered composite containing an embedded penny-shaped crack and subjected to normal and radial impact. The material properties of the layers are chosen such that the crack lies in a layer of matrix material while the surrounding material possesses the average elastic properties of a two-phase medium consisting of a large number of fibers embedded in the matrix. Quantitatively, the time-dependent stresses near the crack border can be described by the dynamic stress intensity factors. Their magnitude depends on time, on the material properties of the composite and on the relative size of the crack compared to the composite local geometry. Results obtained show that, for the same material properties and geometry of the composite, the dynamic stress intensity factors for an embedded (penny-shaped) crack reach their peak values within a shorter period of time and with a lower magnitude than the corresponding dynamic stress intensity factors for a through-crack.			
17. Key Words (Suggested by Author(s)) Composites, normal impact, radial impact penny-shaped crack, elastodynamics, stress analysis, stress intensity, Laplace transform, Fourier transform, Fredholm integral equations.		18. Distribution Statement Unclassified	
19. Security Classif. (of this report) Unclassified	20. Security Classif. (of this page) Unclassified	21. No. of Pages 33	22. Price*

*For sale by the National Technical Information Service, Springfield, Virginia 22161

FOREWORD

This research work deals with the normal and radial impact of composites with embedded penny-shaped cracks which represents a portion of the program supported by the NASA-Lewis Research Center in Cleveland, Ohio. The program covers the period from February 13, 1978 to February 12, 1979 under Grant NSG 3179 and is conducted by the Institute of Fracture and Solid Mechanics at Lehigh University.

Professor George C. Sih served as the Principal Investigator while Dr. E. P. Chen was the Associate Investigator who is now employed by the Sandia Laboratory in New Mexico. The capable guidance of Dr. Christos C. Chamis who acted as the NASA Project Manager is very much appreciated. His encouragement has led to the success of this work.

TABLE OF CONTENTS

FOREWORD	iv
TABLE OF CONTENTS	v
LIST OF FIGURES	vi
LIST OF SYMBOLS	
ABSTRACT	1
INTRODUCTION	2
AXIAL SYMMETRIC DEFORMATION: PENNY-SHAPED CRACK	3
NORMAL IMPACT	7
<i>Fredholm integral equations</i>	8
<i>Stress intensity factor for normal impact</i>	9
RADIAL IMPACT	11
<i>Integral equations</i>	12
<i>Stress intensity factor for radial impact</i>	14
CONCLUDING REMARKS	15
APPENDIX: EXPRESSIONS FOR $A^{(i)}(s,p), \dots, C^{(i)}(s,p)$	16
<i>Radial impact</i>	18
ACKNOWLEDGEMENTS	19
REFERENCES	19
FIGURES	21
COMPUTER PROGRAMS	
<i>Axial impact</i>	34
<i>Torsional impact</i>	41

LIST OF FIGURES

Figure 1 - Penny-shaped crack embedded in a matrix layer under normal and radial impact	21
Figure 2 - Plot of $\Lambda_I^*(1,p)$ versus c_{21}/pa for $a/b = 1.0$	22
Figure 3 - Plot of $\Lambda_I^*(1,p)$ versus c_{21}/pa for $\mu_2/\mu_1 = 0.1$	23
Figure 4 - Plot of $\Lambda_I^*(1,p)$ versus c_{21}/pa for $\mu_2/\mu_1 = 10.0$	24
Figure 5 - Dynamic stress intensity factor $k_1(t)$ for penny-shaped crack with $a/b = 1.0$	25
Figure 6 - Dynamic stress intensity factor $k_1(t)$ for penny-shaped crack with $\mu_2/\mu_1 = 0.1$	26
Figure 7 - Dynamic stress intensity factor $k_1(t)$ for penny-shaped crack with $\mu_2/\mu_1 = 10.0$	27
Figure 8 - Variations of $\Lambda_{II}^*(1,p)$ with c_{21}/pa for $a/b = 1.0$	28
Figure 9 - Variations of $\Lambda_{II}^*(1,p)$ with c_{21}/pa for $\mu_2/\mu_1 = 0.1$ and varying a/b	29
Figure 10 - Variations of $\Lambda_{II}^*(1,p)$ with c_{21}/pa for $\mu_2/\mu_1 = 10$ and varying a/b	30
Figure 11 - Stress intensity factor $k_2(t)$ versus time for a penny-shaped crack with $a/b = 1.0$	31
Figure 12 - Stress intensity factor $k_2(t)$ versus time for a penny-shaped crack with $\mu_2/\mu_1 = 0.1$	32
Figure 13 - Stress intensity factor $k_2(t)$ versus time for a penny-shaped crack with $\mu_2/\mu_1 = 10.0$	33

LIST OF SYMBOLS

a	- radius of crack
$A(s,p), B(s,p)$	- unknowns in dual integral equations
$A^{(i)}, B^{(i)}, C^{(i)}$	- coefficients for transform of solution, functions of (s,p)
b	- half of the thickness of the layer
Br	- Bromwich contour in the complex p -plane
c_{1j}, c_{2j}	- dilatational and shear wave speeds for medium j
$e^{(i)}$	- functions of (p,s) through γ_{ij}
$f^*(p)$	- Laplace transform of $f(t)$
$f^h(s)$	- Hankel transform of $f(x)$
$(f)_j$	- indicates that f is evaluated in medium j
$h(t)$	- Heaviside unit step function
$J_n(x)$	- Bessel function of order n
$k_1(t), k_2(t)$	- dynamic stress intensity factors
$M_I(\xi, n, p)$	- kernel of Fredholm integral equation
$M_{II}(\xi, n, p)$	- kernel of Fredholm integral equation
$P_I(s,p), P_{II}(s,p)$	- kernel in dual integral equations
r, θ, z	- cylindrical coordinates
r_1, θ_1	- crack tip polar coordinates
u_r, u_θ	- displacement components
t	- time
x, y, z	- rectangular coordinates - crack lies in the xy -plane
γ_{ij}	- exponents for transform of solution, functions of (p,s)
$\delta^{(i)}$	- functions of (p,s) through $e^{(i)}$
Δ_I, Δ_{II}	- functions of (p,s) through $\delta^{(i)}$
λ_1, λ_2	- Lamé coefficient

$\Lambda_I^*(\xi, p), \Lambda_{II}^*(\xi, p)$	- unknown in Fredholm integral equation
μ_1, μ_2	- shear modulus
ν_1, ν_2	- Poisson's ratio
ρ_1, ρ_2	- mass density
σ_0	- suddenly applied normal stress
$\sigma_r, \sigma_\theta, \sigma_z, \tau_{rz}$	- stress components
τ_0	- suddenly applied shear stress
ϕ_j, ψ_j	- scalar potentials for medium j
∇^2	- Laplacian operator

NORMAL AND RADIAL IMPACT OF COMPOSITES
WITH EMBEDDED PENNY-SHAPED CRACKS

by

G. C. Sih
Institute of Fracture and Solid Mechanics
Lehigh University
Bethlehem, Pennsylvania 18015

and

E. P. Chen*
Sandia Laboratories
Albuquerque, New Mexico 87115

ABSTRACT

A method is developed for the dynamic stress analysis of a layered composite containing an embedded penny-shaped crack and subjected to normal and radial impact. The material properties of the layers are chosen such that the crack lies in a layer of matrix material while the surrounding material possesses the average elastic properties of a two-phase medium consisting of a large number of fibers embedded in the matrix. Quantitatively, the time-dependent stresses near the crack border can be described by the dynamic stress intensity factors. Their magnitude depends on time, on the material properties of the composite and on the relative size of the crack compared to the composite local geometry. Results obtained show that, for the same material properties and geometry of the composite, the dynamic stress intensity factors for an embedded (penny-shaped) crack reach their peak values within a shorter period of time and with a lower magnitude than the corresponding dynamic stress factors for a through-crack.

*This work was completed when Dr. Chen was a faculty member at Lehigh University.

INTRODUCTION

Advanced composite materials are multi-phased nonhomogeneous materials with anisotropic properties. This complicates the stress analysis for fracture, particularly if the loading is time-dependent and the geometry involves sharp edges such as a crack. As a result, conventional and mathematical techniques for dynamic fracture generally fail to yield accurate results.

An effective approach for finding dynamic stresses in a nonhomogeneous composite containing a through crack has been developed [1] by utilizing both the Laplace and Fourier transforms. The transient boundary, symmetry and continuity conditions were formulated by integral representations in terms of the rectangular Cartesian coordinates x and y and the results for the stress intensity factors are determined numerically by solving a standard integral equation in the Laplace transform plane. The crack geometry was assumed to be extended infinitely in the z -direction or through the side wall of the composite specimen. Many of the failures in composites, however, were observed [2] to initiate from embedded mechanical imperfections such as air bubbles, voids or cavities. Hence, a more realistic modeling of the actual flaw geometry would be an embedded crack that has finite dimensions in all directions. This immediately suggests a three-dimensional elastodynamic crack problem which cannot be solved effectively by analytical means unless symmetry prevails. One approach for obtaining a solution is to extend the integral transform formulation for a through crack in rectangular coordinates [1] to that of an embedded crack in cylindrical polar coordinates. This necessitates the use of Hankel transforms instead of Fourier transforms.

Although no attempt will be made to analyze the failure of the composite due to impact, the dynamic stress intensity factors $k_1(t)$ and $k_2(t)$ can be readily

used in a given fracture criterion, say the strain energy density theory [3], for determining the allowable level of impact load. The new results can also assist the construction of composite materials for establishing impact tolerance. In this case, failure is assumed to initiate from a damage zone of material in the composite that can be approximated by an embedded crack. The time-dependent characteristics of the stresses for the through and embedded crack geometries are compared and studied for different elastic properties and dimensions of the composite. In particular, the phenomenon of elastic waves reflecting from the crack to the interfaces within the composite can be exhibited numerically when their neighboring boundaries are sufficiently close to one another. As time becomes very large, all of the results in this report reduce to the corresponding static solutions [4].

AXIAL SYMMETRIC DEFORMATION: PENNY-SHAPED CRACK

Consider a penny-shaped crack of radius a that lies in a layer of material of thickness $2b$ with material properties μ_1 , ν_1 , ρ_1 . This layer is bonded between two media with properties μ_2 , ν_2 , ρ_2 as illustrated in Figure 1. With reference to the system of coordinates (x,y,z) , the z -axis coincides with the center of the crack and is normal to the crack situated in the xy -plane. The outer boundaries of the composite are assumed to be sufficiently far away from the crack such that the reflected waves will have a negligible influence on the local stresses. Only those impact loads that produce an axisymmetric wave pattern will be considered.

For an axially symmetric deformation field, material elements are displaced only in the radial and axial direction and remain unchanged in the θ -direction. With reference to the cylindrical polar coordinates (r,θ,z) in Figure 1, the

two nonzero displacement components can be expressed in terms of the wave potentials $\phi_j(r, z, t)$ and $\psi_j(r, z, t)$ as follows:

$$(u_r)_j = \frac{\partial \phi_j}{\partial r} - \frac{\partial \psi_j}{\partial z} \quad (1)$$

$$(u_z)_j = \frac{\partial \phi_j}{\partial z} + \frac{\partial \psi_j}{\partial r} - \frac{\psi_j}{r}$$

where $j = 1$ refers to the layer with the crack and $j = 2$ to the surrounding material. The four nontrivial stress components are given by

$$\begin{aligned} (\sigma_r)_j &= 2\mu_j \frac{\partial}{\partial r} \left(\frac{\partial \phi_j}{\partial r} - \frac{\partial \psi_j}{\partial z} \right) + \lambda_j \nabla^2 \phi_j \\ (\sigma_\theta)_j &= 2\mu_j \frac{1}{r} \left(\frac{\partial \phi_j}{\partial r} - \frac{\partial \psi_j}{\partial z} \right) + \lambda_j \nabla^2 \phi_j \\ (\sigma_z)_j &= 2\mu_j \frac{\partial}{\partial z} \left(\frac{\partial \phi_j}{\partial z} + \frac{\partial \psi_j}{\partial r} + \frac{\psi_j}{r} \right) + \lambda_j \nabla^2 \phi_j \\ (\tau_{rz})_j &= \mu_j \left[\frac{\partial}{\partial z} \left(2 \frac{\partial \phi_j}{\partial r} - \frac{\partial \psi_j}{\partial z} \right) + \frac{\partial}{\partial r} \left(\frac{\partial \phi_j}{\partial r} + \frac{\psi_j}{r} \right) \right] \end{aligned} \quad (2)$$

in which λ_j and μ_j are the Lamé constants and ∇^2 represents the operator

$$\nabla^2 = \frac{\partial^2}{\partial r^2} + \frac{1}{r} \frac{\partial}{\partial r} + \frac{\partial^2}{\partial z^2}$$

The governing equations can thus be obtained from the equations of motion which yield

$$\frac{\partial^2 \phi_j}{\partial r^2} + \frac{1}{r} \frac{\partial \phi_j}{\partial r} + \frac{\partial^2 \phi_j}{\partial z^2} = \frac{1}{c_{1j}^2} \frac{\partial^2 \phi_j}{\partial t^2} \quad (3)$$

$$\frac{\partial^2 \psi_j}{\partial r^2} + \frac{1}{r} \frac{\partial \psi_j}{\partial r} - \frac{\psi_j}{r^2} + \frac{\partial^2 \psi_j}{\partial z^2} = \frac{1}{c_{2j}^2} \frac{\partial^2 \psi_j}{\partial t^2}$$

with c_{1j} and c_{2j} being the dilatational and shear wave speeds:

$$c_{1j} = \left(\frac{\lambda_j + 2\mu_j}{\rho_j} \right)^{1/2}, \quad c_{2j} = \left(\frac{\mu_j}{\rho_j} \right)^{1/2} \quad (4)$$

If the composite body is initially at rest, the Laplace transform of equations (3) further give

$$\frac{\partial^2 \phi_j^*}{\partial r^2} + \frac{1}{r} \frac{\partial \phi_j^*}{\partial r} + \frac{\partial^2 \phi_j^*}{\partial z^2} = \frac{p^2}{c_{1j}^2} \phi_j^* \quad (5)$$

$$\frac{\partial^2 \psi_j^*}{\partial r^2} + \frac{1}{r} \frac{\partial \psi_j^*}{\partial r} - \frac{\psi_j^*}{r^2} + \frac{\partial^2 \psi_j^*}{\partial z^2} = \frac{p^2}{c_{2j}^2} \psi_j^*$$

Here, p is the transform variable in the Laplace transform pair:

$$f^*(p) = \int_0^\infty f(t) \exp(-pt) dt \quad (6)$$

$$f(t) = \frac{1}{2\pi i} \int_{Br} f^*(p) \exp(pt) dp$$

The abbreviation Br stands for the Bromwich path of integration. Moreover, since the composite geometry is symmetrical about the xy -plane, it suffices to consider

only the solution in the upper half-space, $z \geq 0$. For the penny-shape crack geometry, the Hankel transform pair [5] may be used:

$$f^h(s) = \int_0^\infty x f(x) J_n(sx) dx \quad (7)$$

$$f(x) = \int_0^\infty s f^h(s) J_n(sx) ds$$

where J_n is the n th order Bessel function of the first kind. Applying equations (7) to (5), the following results are obtained:

$$\phi_1^*(r, z, p) = \int_0^\infty [A^{(1)}(s, p)e^{-\gamma_{11}z} + A^{(2)}(s, p)e^{\gamma_{11}z}] J_0(rs) ds \quad (8)$$

$$\psi_1^*(r, z, p) = \int_0^\infty [B^{(1)}(s, p)e^{-\gamma_{21}z} + B^{(2)}(s, p)e^{\gamma_{21}z}] J_1(rs) ds$$

for the cracked layer and

$$\phi_2^*(r, z, p) = \int_0^\infty C^{(1)}(s, p)e^{-\gamma_{12}z} J_0(rs) ds \quad (9)$$

$$\psi_2^*(r, z, p) = \int_0^\infty C^{(2)}(s, p)e^{-\gamma_{22}z} J_1(rs) ds$$

for the surrounding material. The quantities γ_{ij} are given by

$$\gamma_{1j} = (s^2 + \frac{p^2}{c_{1j}^2})^{1/2}, \quad \gamma_{2j} = (s^2 + \frac{p^2}{c_{2j}^2})^{1/2} \quad (10)$$

The six unknowns $A^{(1)}, A^{(2)}, \dots, C^{(2)}$ are determined from a given set of transient boundary, symmetry and continuity conditions.

NORMAL IMPACT

Let the penny-shaped crack be subjected to a uniform impact load* such that the upper and lower surface will move in the opposite direction. The magnitude of this normal load is σ_0 and since it is applied suddenly from $t = 0$ and maintained at a constant value thereafter, the Heaviside unit step function, $H(t)$, will be used, i.e., $-\sigma_0 H(t)$. Making use of equations (6), the conditions on the plane $z = 0$ for $r \leq a$ and $r \geq a$ take the forms

$$(\sigma_z^*)_1 (r, 0, p) = -\frac{\sigma_0}{p}; (\tau_{rz}^*)_1 (r, 0, p) = 0, 0 \leq r < a \quad (11)$$

$$(\sigma_z^*)_1 (r, 0, p) = 0; (\tau_{rz}^*)_1 (r, 0, p) = 0, r \geq a$$

If the interfaces at $z = \pm b$ is bonded perfectly, the stresses and displacements can then be considered continuous across these planes, i.e.,

$$(\sigma_z^*)_1 (r, b, p) = (\sigma_z^*)_2 (r, b, p) \quad (12)$$

$$(\tau_{rz}^*)_1 (r, b, p) = (\tau_{rz}^*)_2 (r, b, p)$$

*There is no loss in generality in formulating the problem in terms of a uniform step load. The principle of superposition may be used to obtain the solution for general loading from a series of step loading solutions as discussed in [1].

and

$$(u_r^*)_1(r, b, p) = (u_r^*)_2(r, b, p) \quad (13)$$

$$(u_z^*)_1(r, b, p) = (u_z^*)_2(r, b, p)$$

Under these considerations, the six functions $A^{(1)}, A^{(2)}, \dots, C^{(2)}$ may be expressed in terms of a single unknown $A(s, p)$ as indicated by equations (A.1) in the Appendix.

Fredholm integral equations. Without going into details, the function $A(s, p)$ can be obtained from the system of dual integral equations

$$\int_0^\infty A(s, p) J_0(rs) ds = 0, \quad r \geq a \quad (14)$$

$$\int_0^\infty s P_I(s, p) A(s, p) J_0(rs) ds = - \frac{\sigma_0}{2\mu_1(1-\kappa_1^2)p}, \quad r < a$$

in which $P_I(s, p)$ is a known function:

$$\begin{aligned} P_I(s, p) = & \frac{1}{s\Delta_I(1-\kappa_1^2)} \left\{ \left[\frac{1}{4} (s^2 + \gamma_{21}^2)^2 - s^2 \gamma_{11} \gamma_{21} \right] [\delta^{(2)} - \delta^{(3)} e^{-2(\gamma_{11} + \gamma_{21})b}] \right. \\ & + s(s^2 + \gamma_{21}^2) e^{-(\gamma_{11} + \gamma_{21})b} [\gamma_{21} (\delta^{(1)} \delta^{(4)} - \delta^{(2)} \delta^{(3)}) - \gamma_{11}] \\ & \left. + \left[\frac{1}{4} (s^2 + \gamma_{21}^2)^2 + s^2 \gamma_{11} \gamma_{21} \right] [\delta^{(4)} e^{-2\gamma_{21}b} - \delta^{(1)} e^{-2\gamma_{11}b}] \right\} \end{aligned} \quad (15)$$

The form of $A(s,p)$ that satisfies equations (14) can be found from Copson [6]:

$$A(s,p) = -\sqrt{\frac{2s}{\pi}} \frac{\sigma_0 a^{5/2}}{2\mu_1 p(1-k_1^2)} \int_0^1 \sqrt{\xi} \Lambda_I^*(\xi,p) J_{1/2}(sa\xi) d\xi \quad (16)$$

Here, $J_{1/2}$ is the half order Bessel function of the first kind and $\Lambda_I^*(\xi,p)$ satisfies the Fredholm integral equation

$$\Lambda_I^*(\xi,p) + \int_0^1 \Lambda_I^*(\eta,p) M_I(\xi,\eta,p) d\eta = \xi \quad (17)$$

whose kernel

$$\begin{aligned} M_I(\xi,\eta,p) &= \sqrt{\xi\eta} \int_0^\infty s [P_I(\frac{s}{a},p) - 1] J_{1/2}(s\xi) J_{1/2}(sn) ds \\ &= \frac{2}{\pi} \int_0^\infty [P_I(\frac{s}{a},p) - 1] \sin(s\xi) \sin(sn) ds \end{aligned} \quad (18)$$

is symmetric in ξ and η . Figures 2 to 4 show the numerical results of equation (17) by varying μ_2/μ_1 and a/b while $\rho_1 = \rho_2$ and $v_1 = v_2 = 0.29$ are kept the same for all cases. The function $\Lambda_I^*(\xi,p)$ evaluated at the crack border, $\xi = 1$, governs the contribution of the geometric and material parameters on $k_1^*(p)$ which represents the Laplace transform of the stress intensity factor.

Stress intensity factor for normal impact. In order to evaluate $k_1^*(p)$ or $k_1(t)$, the stresses in the matrix layer are first expanded in terms of the local coordinates r_1 and θ_1 for small values of r_1 . The local coordinates (r_1, θ_1) are related to (r, θ) in Figure 1 as follows:

$$a + r_1 \cos\theta_1 = r \cos\theta \quad (19)$$

$$r_1 \sin\theta_1 = r \sin\theta$$

The leading term in the Laplace transform of the local stresses that possess the $1/\sqrt{r_1}$ singularity is

$$k_1^*(p) = \frac{\Lambda_I^*(1, p)}{p} \frac{2}{\pi} \sigma_0 \sqrt{a} \quad (20)$$

Application of the Laplace inversion theorem yields the dynamic stress field around the crack border as a function of time. The result is

$$\begin{aligned} (\sigma_r)_1(r_1, \theta_1, t) &= \frac{k_1(t)}{\sqrt{2r_1}} \cos \frac{\theta_1}{2} (1 - \sin \frac{\theta_1}{2} \sin \frac{3\theta_1}{2}) + O(r_1^0) \\ (\sigma_\theta)_1(r_1, \theta_1, t) &= \frac{k_1(t)}{\sqrt{2r_1}} 2v_1 \cos \frac{\theta_1}{2} + O(r_1^0) \\ (\sigma_z)_1(r_1, \theta_1, t) &= \frac{k_1(t)}{\sqrt{2r_1}} \cos \frac{\theta_1}{2} (1 + \sin \frac{\theta_1}{2} \sin \frac{3\theta_1}{2}) + O(r_1^0) \\ (\tau_{rz})_1(r_1, \theta_1, t) &= \frac{k_1(t)}{\sqrt{2r_1}} \cos \frac{\theta_1}{2} \sin \frac{\theta_1}{2} \cos \frac{3\theta_1}{2} + O(r_1^0) \end{aligned} \quad (21)$$

and $k_1(t)$ becomes

$$k_1(t) = \frac{2\sigma_0 \sqrt{a}}{\pi} \frac{1}{2\pi i} \int_{Br} \frac{\Lambda_I^*(1, p)}{p} e^{pt} dp \quad (22)$$

Note that equation (20) is, in fact, the Laplace transform of equation (22). Hence, the functional dependence of r_1 and θ_1 is not affected by the Laplace

transformation and can be evaluated separately. This observation was first made by Sih, Ravera and Embley [7].

Making use of the results for $\Lambda_I^*(1,p)$ in Figures 2 to 4, $k_1(t)$ in equation (22) can be found as given in Figures 5 to 7. The dynamic stress intensity factors $k_1(t)$ for the penny-shaped crack exhibit an oscillatory behavior rising quickly to a peak. As time increases, all curves approach the static value of $k_1 = 2\sigma_0\sqrt{a}/\pi$ [4]. For a crack diameter to layer thickness ratio of $a/b = 1$, the peaks of the $k_1(t)$ curve are sensitive to changes in the shear moduli ratio μ_2/μ_1 . Figure 5 indicates that $k_1(t)$ tends to decrease in amplitude as μ_2/μ_1 is reduced from 0.1 to 10.0. The influence of the composite interface on $k_1(t)$ is exhibited in Figures 6 to 7. When the shear modulus of the surrounding material μ_2 is much smaller than the matrix layer with μ_1 , the dynamic crack border stress intensity increases as the crack diameter becomes large in comparison with the layer thickness. This effect is clearly evidenced in Figure 6. As expected, $k_1(t)$ increases with decreasing a/b when the shear modulus of the cracked layer is made smaller than the surrounding material, i.e., $\mu_1 < \mu_2$ as illustrated in Figure 7. The result of Embley and Sih [8] is recovered for the homogeneous case, $\mu_1 = \mu_2$.

RADIAL IMPACT

If the penny-shaped crack is sheared uniformly in the radial direction such that axial symmetry is preserved, then $\phi_j^*(r,z,p)$ and $\psi_j^*(r,z,p)$ in equations (8) and (9) remain valid. Let this shear of magnitude τ_0 be applied suddenly and hence the surface tractions, $-\tau_0 H(t)$, are to be specified for $0 \leq r < a$ with $H(t)$ being the Heaviside unit step function. Laplace transform of the conditions on the plane $z = 0$ thus become

$$(\tau_{rz}^*)_1(r, o, p) = -\frac{\tau_0}{p}; (\sigma_z^*)_1(r, o, p) = 0, 0 \leq r < a$$

(23)

$$(u_r^*)_1(r, o, p) = 0; (\sigma_z^*)_1(r, o, p) = 0, r \geq a$$

Continuity of the stresses across the interface $z = b$ is satisfied if

$$(\sigma_z^*)_1(r, b, p) = (\sigma_z^*)_2(r, b, p)$$

(24)

$$(\sigma_{rz}^*)_1(r, b, p) = (\sigma_{rz}^*)_2(r, b, p)$$

and the same requirement is imposed on the displacements:

$$(u_r^*)_1(r, b, p) = (u_r^*)_2(r, b, p)$$

(25)

$$(u_z^*)_1(r, b, p) = (u_z^*)_2(r, b, p)$$

Integral equations. As in the case of normal impact, the six unknown functions $A^{(1)}(s, p)$, $A^{(2)}(s, p)$, ..., $C^{(2)}(s, p)$ in equations (8) and (9) can be expressed in terms of a single unknown $B(s, p)$. Refer to equations (A.5) in the Appendix. Hence, equations (24) and (25) are satisfied. The remaining boundary conditions in equations (23) are employed to obtain the system of dual integral equations

$$\int_0^\infty B(s, p) J_1(rs) ds = 0, \quad r \geq a \quad (26)$$

$$\int_0^\infty s P_{II}(s, p) B(s, p) J_1(rs) ds = - \frac{\tau_0}{2\mu_1(1-\kappa_1^2)p}, \quad r < a$$

in which

$$P_{II}(s, p) = \frac{\Delta_I}{\Delta_{II}} P_I(s, p) \quad (27)$$

where $P_I(s, p)$ is already known through equation (15) while $\Delta_I(s, p)$ and $\Delta_{II}(s, p)$ are given by equations (A.2) and (A.6), respectively.

Solving for $B(s, p)$ [6], it can be shown that

$$B(s, p) = - \sqrt{\frac{\pi s}{2}} \frac{\tau_0 a^{5/2}}{4\mu_1 p(1-\kappa_1^2)} \int_0^1 \sqrt{\xi} \Lambda_{II}^*(\xi, p) J_{3/2}(sa\xi) d\xi \quad (28)$$

and $\Lambda_{II}^*(\xi, p)$ satisfies the Fredholm integral equation of the second kind:

$$\Lambda_{II}^*(\xi, p) + \int_0^1 \Lambda_{II}^*(\eta, p) M_{II}(\xi, \eta, p) d\eta = \xi \quad (29)$$

whose kernel takes the form

$$M_{II}(\xi, \eta, p) = \sqrt{\xi\eta} \int_0^\infty s [P_{II}(\frac{s}{a}, p) - 1] J_{3/2}(s\xi) J_{3/2}(s\eta) ds \quad (30)$$

Plots of $\Lambda_{II}^*(1, p)$ as a function of c_{21}/pa are shown in Figures 8 to 10 for different values of μ_2/μ_1 and a/h . The curves show that $\Lambda_{II}^*(1, p)$ rises rapidly at first and then levels off.

Stress intensity factor for radial impact. The dynamic crack border stress field corresponding to radial shear can be obtained in the same way and expressed in terms of the coordinates (r_1, θ_1) in equations (19):

$$\begin{aligned}
 (\sigma_r)_1(r_1, \theta_1, t) &= \frac{k_2(t)}{\sqrt{2r_1}} \sin \frac{\theta_1}{2} (2 + \cos \frac{\theta_1}{2} \cos \frac{3\theta_1}{2}) + O(r_1^\circ) \\
 (\sigma_\theta)_1(r_1, \theta_1, t) &= \frac{k_2(t)}{\sqrt{2r_1}} 2v_1 \sin \frac{\theta_1}{2} + O(r_1^\circ) \\
 (\sigma_z)_1(r_1, \theta_1, t) &= - \frac{k_2(t)}{\sqrt{2r_1}} \sin \frac{\theta_1}{2} \cos \frac{\theta_1}{2} \cos \frac{3\theta_1}{2} + O(r_1^\circ) \\
 (\tau_{rz})_1(r_1, \theta_1, t) &= \frac{k_2(t)}{\sqrt{2r_1}} \cos \frac{\theta_1}{2} (1 - \sin \frac{\theta_1}{2} \sin \frac{3\theta_1}{2}) + O(r_1^\circ)
 \end{aligned} \tag{31}$$

Note that $k_2(t)$ can be evaluated from

$$k_2(t) = \frac{\tau_0 \sqrt{a}}{4\pi i} \int_{Br} \frac{\Lambda_{II}^*(1, p)}{p} e^{pt} dp \tag{32}$$

once $\Lambda_{II}^*(1, p)$ as given by Figures 8 to 10 is known.

The numerical results in Figures 11 to 13 for $k_2(t)$ as a function of time refer to $\rho_1 = \rho_2$ and $v_1 = v_2 = 0.29$. The curve with $\mu_1 = \mu_2$ is the solution for the homogeneous material treated previously by Embley and Sih [8]. In general, $k_2(t)$ oscillates with time and can be greater or smaller than the corresponding homogeneous solution depending on whether $\mu_2/\mu_1 < 1$ or $\mu_2/\mu_1 > 1$. Figure 11 displays the variations of $k_2(t)$ for different values of μ_2/μ_1 while a/b is fixed at unity. The influence of the ratio of crack size with layer thickness

is exhibited in Figures 12 and 13 for $\mu_2/\mu_1 = 0.1$ and $\mu_2/\mu_1 = 10.0$, respectively. These two cases show the opposite effect which is to be expected.

CONCLUDING REMARKS

The previous discussion has shown that the dynamic stress intensity factors for an embedded crack can be evaluated analytically by a method similar to that developed for a through crack [1]. An important consideration is to compare the results for these two crack configurations and to draw some general conclusions. First of all, the $k_1(t)$ or $k_2(t)$ factor for the penny-shaped crack tends to rise more quickly than the through crack, i.e., the peak value of $k_1(t)$ or $k_2(t)$ is reached within a shorter period of time. This is because waves emanating from the neighboring points on the periphery of the penny-shaped crack interfere with each other much earlier as compared to a line (or plane) crack where the waves must travel from one end to the other before interference can take place. In general, the maximum value of $k_1(t)$ or $k_2(t)$ for an embedded crack is lower than that for a through crack. For example, Figure 5 gives a peak value of approximately 1.6 for $\pi k_1(t)/2\sigma_0\sqrt{a}$ which corresponds to $a/b = 1.0$ and $\mu_2/\mu_1 = 0.1$. This occurs at $c_{21}t/a \approx 1.6$ and yields $k_1(t) \approx 1.02 \sigma_0\sqrt{a}$. The corresponding case of a through crack [1] renders $k_1(t) \approx 2.40 \sigma_0\sqrt{a}$ and $c_{21}t/a \approx 3.0$. The difference in $k_1(t)$ is more than a factor of two and is more pronounced as the ratio a/b is increased. For embedded cracks that are non-circular in shape, approximate estimates of $k_1(t)$ can be made by taking the solution for the through crack as an upper limit and that of the circular crack as a lower limit.

In the absence of axisymmetry, the dynamic stress analysis will become exceedingly difficult and it will be more feasible to solve the crack problem numerically. In such cases, the solutions obtained here can be used to guide the development of numerical procedures.

APPENDIX: EXPRESSIONS FOR $A^{(i)}(s,p), \dots, C^{(i)}(s,p)$

Normal impact. The functions $A^{(1)}(s,p), A^{(2)}(s,p), \dots, C^{(2)}(s,p)$ for the wave potentials in equations (8) and (9) can be expressed in terms of a single unknown $A(s,p)$ for normal impact

$$A^{(1)}(s,p) = \left[\frac{1}{2} (s^2 + \gamma_{21}^2) (\delta^{(2)} + \delta^{(4)} e^{-2\gamma_{21}b}) - s\gamma_{11} e^{-(\gamma_{11} + \gamma_{21})b} \right] \frac{A(s,p)}{\Delta_I}$$

$$A^{(2)}(s,p) = - [s\gamma_{11} e^{-(\gamma_{11} + \gamma_{21})b} + \frac{1}{2} (s^2 + \gamma_{21}^2) e^{-2\gamma_{11}b} (\delta^{(1)} + \delta^{(3)} e^{-2\gamma_{21}b})] \times \frac{A(s,p)}{\Delta_I}$$

$$B^{(1)}(s,p) = - [\delta^{(1)} A^{(1)} e^{-\gamma_{11}b} + \delta^{(2)} A^{(2)} e^{\gamma_{11}b}]$$

$$B^{(2)}(s,p) = - [\delta^{(3)} A^{(1)} e^{-\gamma_{11}b} + \delta^{(4)} A^{(2)} e^{\gamma_{11}b}] \quad (A.1)$$

$$C^{(1)}(s,p) = \frac{e^{\gamma_{12}b}}{s^2 - \gamma_{12}\gamma_{22}} [(s^2 - \gamma_{11}\gamma_{22}) A^{(1)} e^{-\gamma_{11}b} + (s^2 + \gamma_{11}\gamma_{22}) A^{(2)} e^{\gamma_{11}b}] \\ - s(\gamma_{21} - \gamma_{22}) B^{(1)} e^{-\gamma_{21}b} + s(\gamma_{21} + \gamma_{22}) B^{(2)} e^{\gamma_{21}b}]$$

$$C^{(2)}(s,p) = \frac{e^{\gamma_{22}b}}{s^2 - \gamma_{12}\gamma_{22}} [s(\gamma_{12} - \gamma_{11}) A^{(1)} e^{-\gamma_{11}b} + s(\gamma_{11} + \gamma_{12}) e^{\gamma_{11}b}] \\ + (s^2 - \gamma_{21}\gamma_{12}) B^{(1)} e^{-\gamma_{21}b} + (s^2 + \gamma_{21}\gamma_{12}) B^{(2)} e^{\gamma_{21}b}]$$

in which Δ_I stands for

$$\Delta_I(s, p) = \frac{p^2}{2c_{21}^2} \gamma_{11} [\delta^{(2)} + \delta^{(3)} e^{-2(\gamma_{11} + \gamma_{21})b} + \delta^{(4)} e^{-2\gamma_{21}b} + \delta^{(1)} e^{-2\gamma_{11}b}] \quad (A.2)$$

and $\delta^{(1)}, \delta^{(2)}, \dots, \delta^{(4)}$ are further expressed in terms of $e^{(1)}, e^{(2)}, \dots, e^{(8)}$ as the following:

$$\begin{aligned} \delta^{(1)}(s, p) &= (e^{(1)}e^{(6)} - e^{(2)}e^{(7)})/(e^{(1)}e^{(6)} - e^{(2)}e^{(5)}) \\ \delta^{(2)}(s, p) &= (e^{(4)}e^{(6)} - e^{(2)}e^{(8)})/(e^{(1)}e^{(6)} - e^{(2)}e^{(5)}) \\ \delta^{(3)}(s, p) &= (e^{(1)}e^{(7)} - e^{(3)}e^{(5)})/(e^{(1)}e^{(6)} - e^{(2)}e^{(5)}) \\ \delta^{(4)}(s, p) &= (e^{(1)}e^{(8)} - e^{(4)}e^{(5)})/(e^{(1)}e^{(6)} - e^{(2)}e^{(5)}) \end{aligned} \quad (A.3)$$

The quantities in equations (A.3) are complicated functions of the materials parameters and transform variables. They are given by

$$\begin{aligned} e^{(1)}(s, p) &= -s\gamma_{21} + \frac{s\mu_2}{\mu_1(s^2 - \gamma_{12}\gamma_{22})} [\frac{1}{2}(\gamma_{21} - \gamma_{22})(s^2 + \gamma_{22}^2) + \gamma_{22}(s^2 - \gamma_{21}\gamma_{12})] \\ e^{(2)}(s, p) &= s\gamma_{21} - \frac{s\mu_2}{\mu_1(s^2 - \gamma_{12}\gamma_{22})} [\frac{1}{2}(\gamma_{21} + \gamma_{22})(s^2 + \gamma_{22}^2) - \gamma_{22}(s^2 + \gamma_{21}\gamma_{12})] \\ e^{(3)}(s, p) &= \frac{1}{2}(s^2 + \gamma_{21}^2) - \frac{\mu_2}{\mu_1(s^2 - \gamma_{12}\gamma_{22})} [\frac{1}{2}(s^2 + \gamma_{22}^2)(s^2 - \gamma_{11}\gamma_{22}) \\ &\quad + s^2\gamma_{22}(\gamma_{11} - \gamma_{12})] \end{aligned}$$

$$\begin{aligned}
e^{(4)}(s, p) &= \frac{1}{2} (s^2 + \gamma_{21}^2) - \frac{\mu_2}{\mu_1(s^2 - \gamma_{12}\gamma_{22})} \left[\frac{1}{2} (s^2 + \gamma_{22}^2)(s^2 + \gamma_{11}\gamma_{22}) \right. \\
&\quad \left. - s^2\gamma_{22}(\gamma_{11} + \gamma_{12}) \right] \\
e^{(5)}(s, p) &= -\frac{1}{2} (s^2 + \gamma_{21}^2) + \frac{\mu_2}{\mu_1(s^2 - \gamma_{12}\gamma_{22})} \left[s^2\gamma_{12}(\gamma_{21} - \gamma_{22}) \right. \\
&\quad \left. + \frac{1}{2} (s^2 + \gamma_{22}^2)(s^2 - \gamma_{21}\gamma_{12}) \right] \\
\end{aligned} \tag{A.4}$$

$$\begin{aligned}
e^{(6)}(s, p) &= -\frac{1}{2} (s^2 + \gamma_{21}^2) - \frac{\mu_2}{\mu_1(s^2 - \gamma_{12}\gamma_{22})} \left[s^2\gamma_{12}(\gamma_{21} + \gamma_{22}) \right. \\
&\quad \left. - \frac{1}{2} (s^2 + \gamma_{22}^2)(s^2 + \gamma_{21}\gamma_{12}) \right]
\end{aligned}$$

$$\begin{aligned}
e^{(7)}(s, p) &= s\gamma_{11} - \frac{s\mu_2}{\mu_1(s^2 - \gamma_{12}\gamma_{22})} \left[\gamma_{12}(s^2 - \gamma_{11}\gamma_{22}) + \frac{1}{2} (s^2 + \gamma_{22}^2)(\gamma_{11} - \gamma_{12}) \right] \\
e^{(8)}(s, p) &= -s\gamma_{11} - \frac{s\mu_2}{\mu_1(s^2 - \gamma_{12}\gamma_{22})} \left[\gamma_{12}(s^2 + \gamma_{11}\gamma_{22}) - \frac{1}{2} (s^2 + \gamma_{22}^2)(\gamma_{11} + \gamma_{12}) \right]
\end{aligned}$$

Radial impact. For radial impact, $A^{(1)}(s, p)$, $A^{(2)}(s, p), \dots, C^{(2)}(s, p)$ in equations (8) and (9) can be expressed in terms of $B(s, p)$ as

$$A^{(1)}(s, p) = -[s\gamma_{21}(\delta^{(2)} - \delta^{(4)}e^{-2\gamma_{21}b}) + \frac{1}{2} (s^2 + \gamma_{21}^2)e^{-(\gamma_{11} + \gamma_{21})b}] \frac{B(s, p)}{\Delta_{II}} \tag{A.5}$$

$$\begin{aligned}
A^{(2)}(s, p) &= [s\gamma_{21}e^{-2\gamma_{11}b}(\delta^{(1)} - \delta^{(3)}e^{-2\gamma_{21}b}) + \frac{1}{2} (s^2 + \gamma_{21}^2)e^{-(\gamma_{11} + \gamma_{21})b}] \\
&\quad \times \frac{B(s, p)}{\Delta_{II}}
\end{aligned}$$

where

$$\Delta_{II} = \frac{p^2}{2c_{21}^2} \gamma_{21} [\delta^{(2)} + \delta^{(3)} e^{-2(\gamma_{11} + \gamma_{21})b} - \delta^{(4)} e^{-2\gamma_{21}b} - \delta^{(1)} e^{-2\gamma_{11}b}] \quad (A.6)$$

The remaining functions $B^{(1)}(s,p)$, $B^{(2)}(s,p)$, etc., can be related to $B(s,p)$ through $A^{(1)}(s,p)$ and $A^{(2)}(s,p)$ since the last four expressions in equations (A.1) for normal impact also apply to radial impact.

ACKNOWLEDGEMENTS

The authors wish to acknowledge the financial support provided by the National Aeronautics and Space Administration, Lewis Research Center, Cleveland, Ohio under Contract No. NSG-3179 with the Institute of Fracture and Solid Mechanics, Lehigh University. They are also grateful to Dr. C. C. Chamis for having expressed an interest in this work.

REFERENCES

- [1] Sih, G. C. and Chen, E. P., "Angle Impact of Unidirectional Composites with Cracks: Dynamic Stress Intensification", Technical Report IFSM No. 95, Lehigh University, January, 1979.
- [2] Lauraitis, K., "Tensile Strength of Off-Axis Unidirectional Composites", University of Illinois TAM Report No. 344, 1971.
- [3] Sih, G. C., "Dynamic Crack Problems: Strain Energy Density Fracture Theory", Mechanics of Fracture, Vol. IV, edited by G. C. Sih, Sijthoff and Noordhoff International Publishing, Alphen, pp. XVII-XLVII, 1977.

- [4] "Three-Dimensional Crack Problems", Mechanics of Fracture, Vol. II, edited by G. C. Sih, Sijthoff and Noordhoff International Publishing, Alphen, Chapter 1, 1975.
- [5] Sneddon, I. N., Fourier Transforms, McGraw-Hill, New York, 1958.
- [6] Copson, E. T., "On Certain Dual Integral Equations", Proceedings of Glasgow Mathematical Association, Vol. 5, pp. 19-24, 1961.
- [7] Sih, G. C., Ravera, R. S. and Embley, G. T., "Impact Response of a Finite Crack in Plane Extension", International Journal of Solids and Structures, Vol. 8, pp. 977-993, 1972.
- [8] Embley, G. T. and Sih, G. C., "Response of a Penny-Shaped Crack to Impact Waves", Proceedings of the 12th Midwestern Mechanics Conference, Vol. 6, pp. 473-487, 1971.

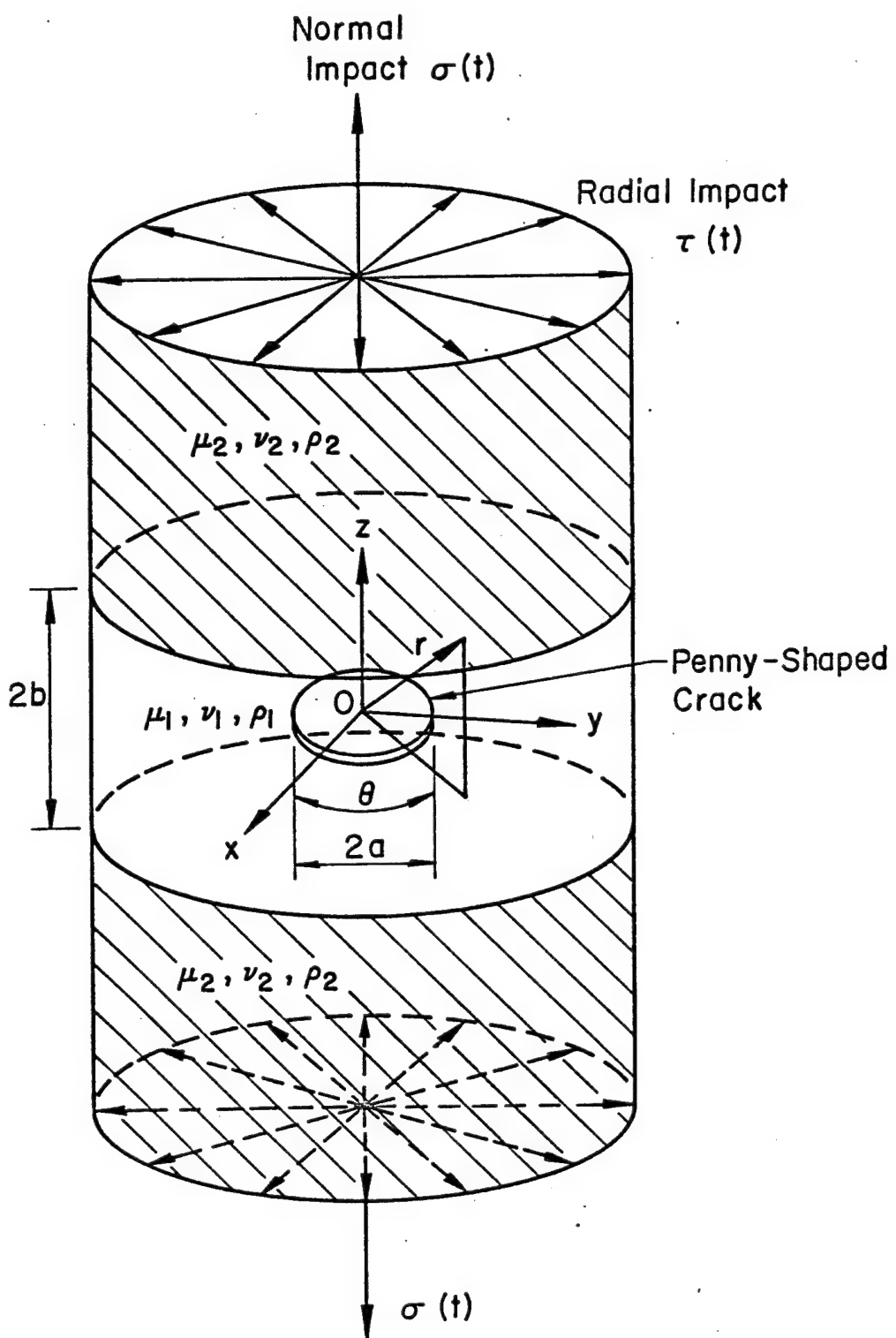


Figure 1 - Penny-shaped crack embedded in a matrix layer under normal and radial impact

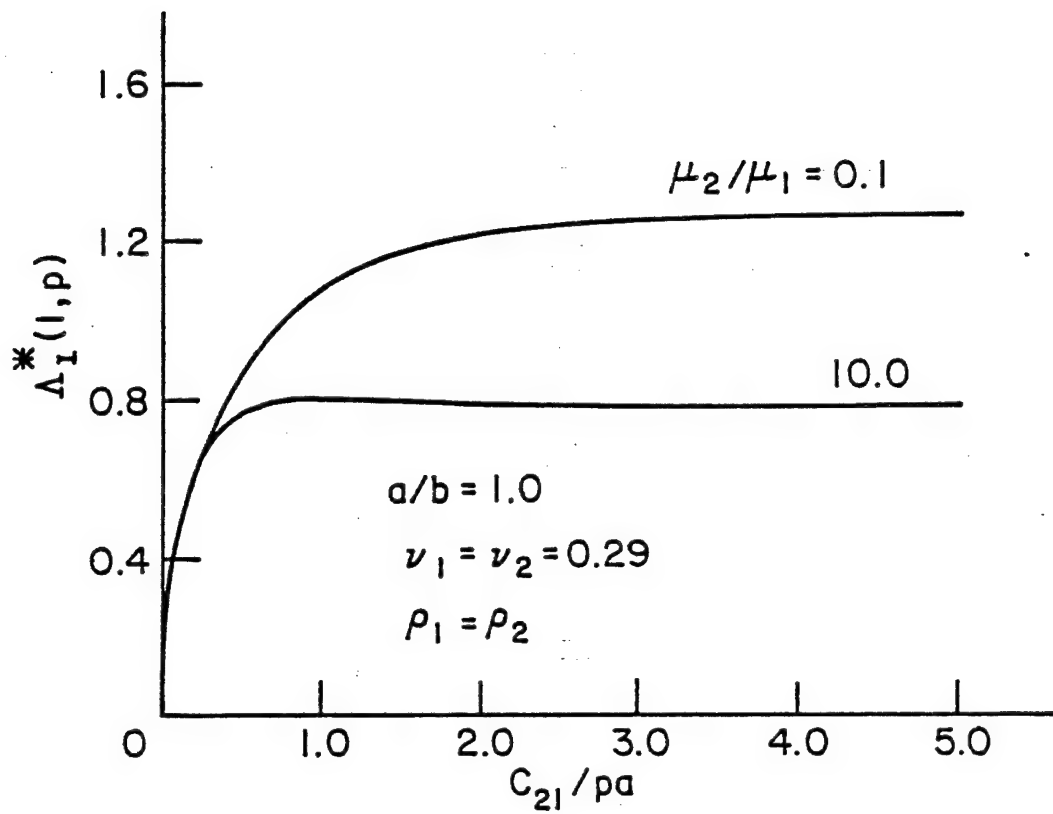


Figure 2 - Plot of $\Lambda_1^*(l, p)$ versus c_{21}/pa for $a/b = 1.0$

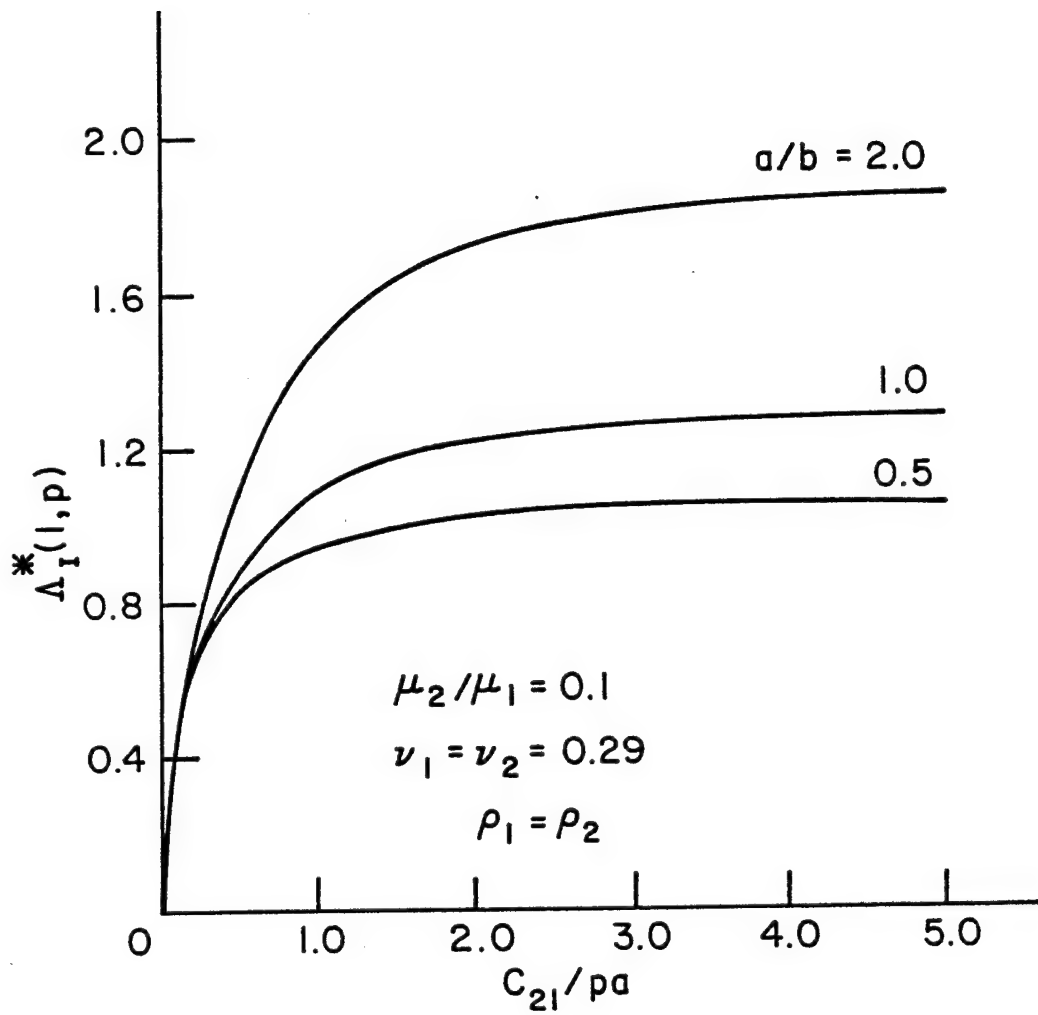


Figure 3 - Plot of $\Lambda_I^*(1,p)$ versus c_{21}/pa for $\mu_2/\mu_1 = 0.1$

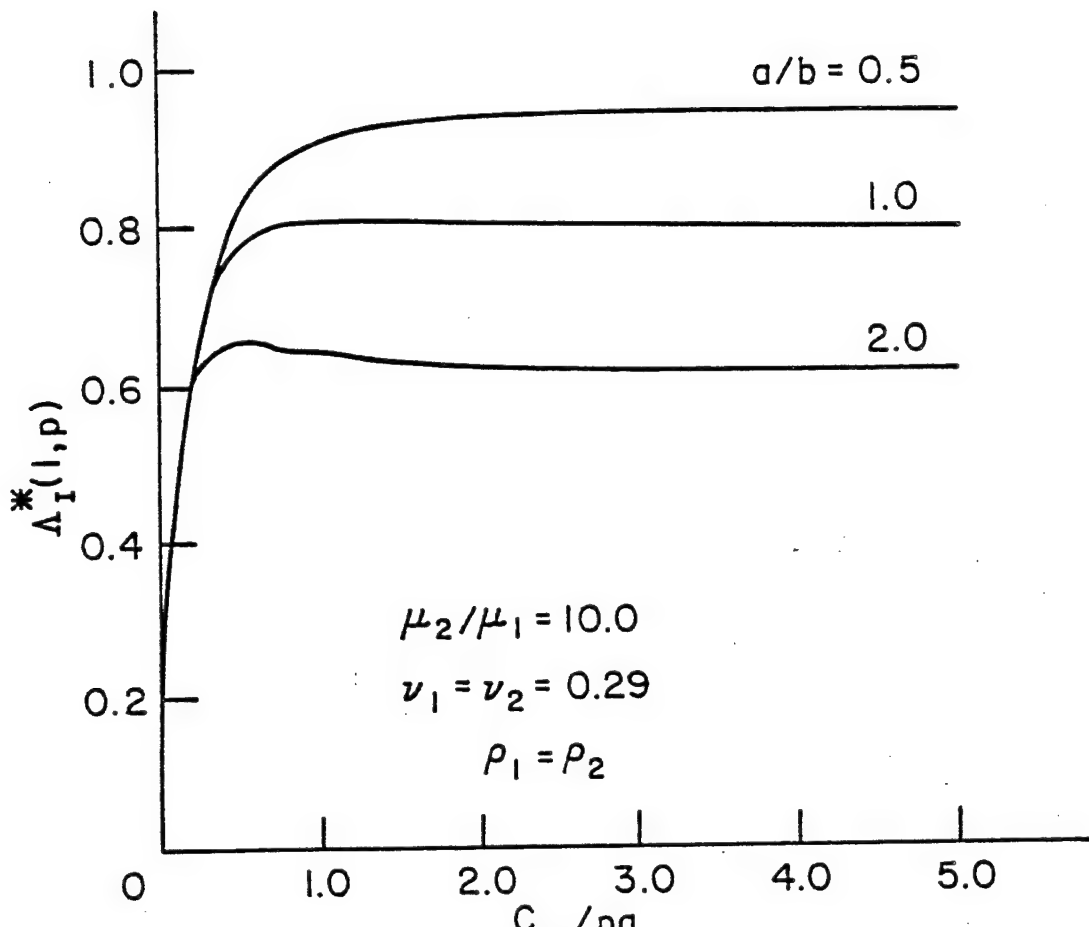


Figure 4 - Plot of $\Lambda_1^*(l, p)$ versus c_{21}/pa for $\mu_2/\mu_1 = 10.0$

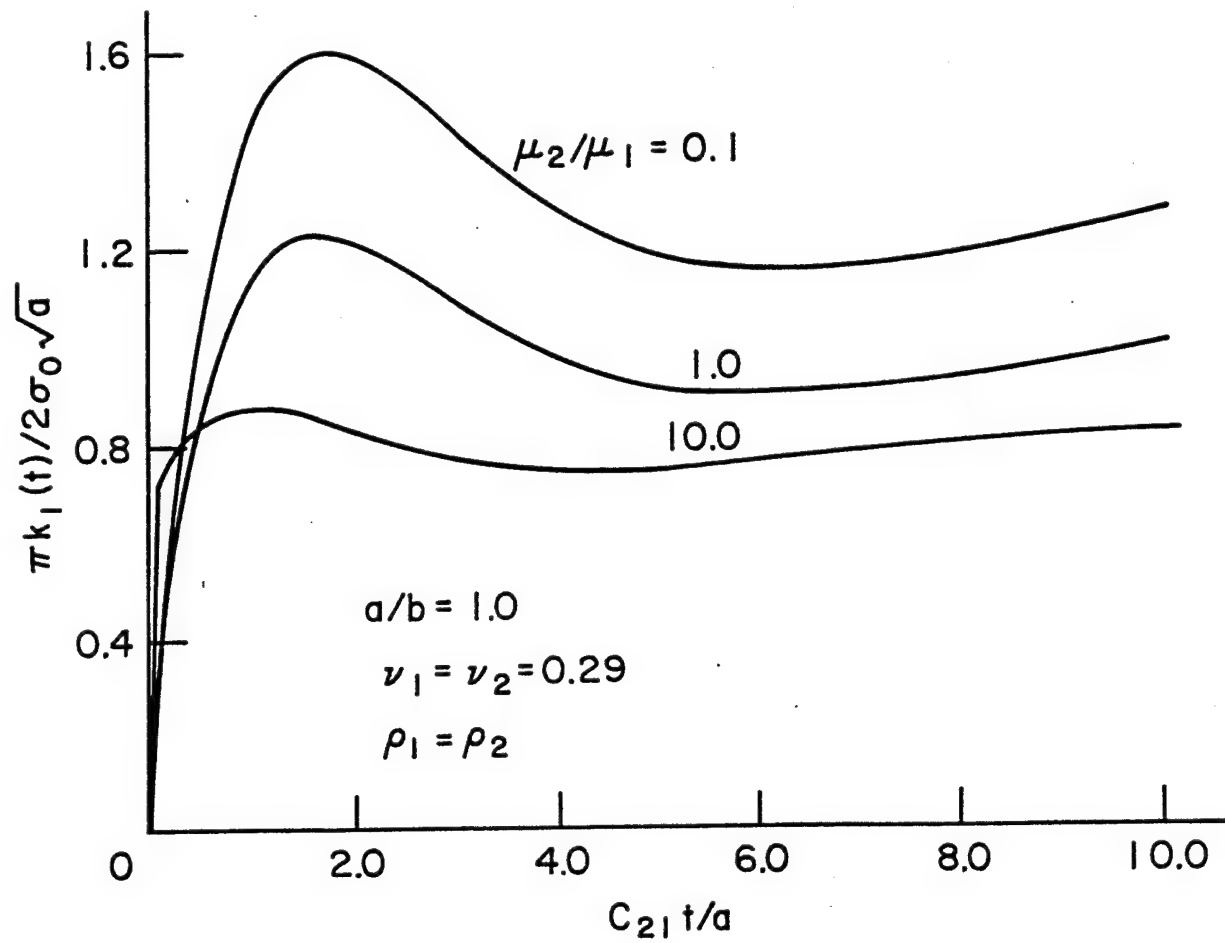


Figure 5 - Dynamic stress intensity factor $k_1(t)$ for penny-shaped crack with $a/b = 1.0$

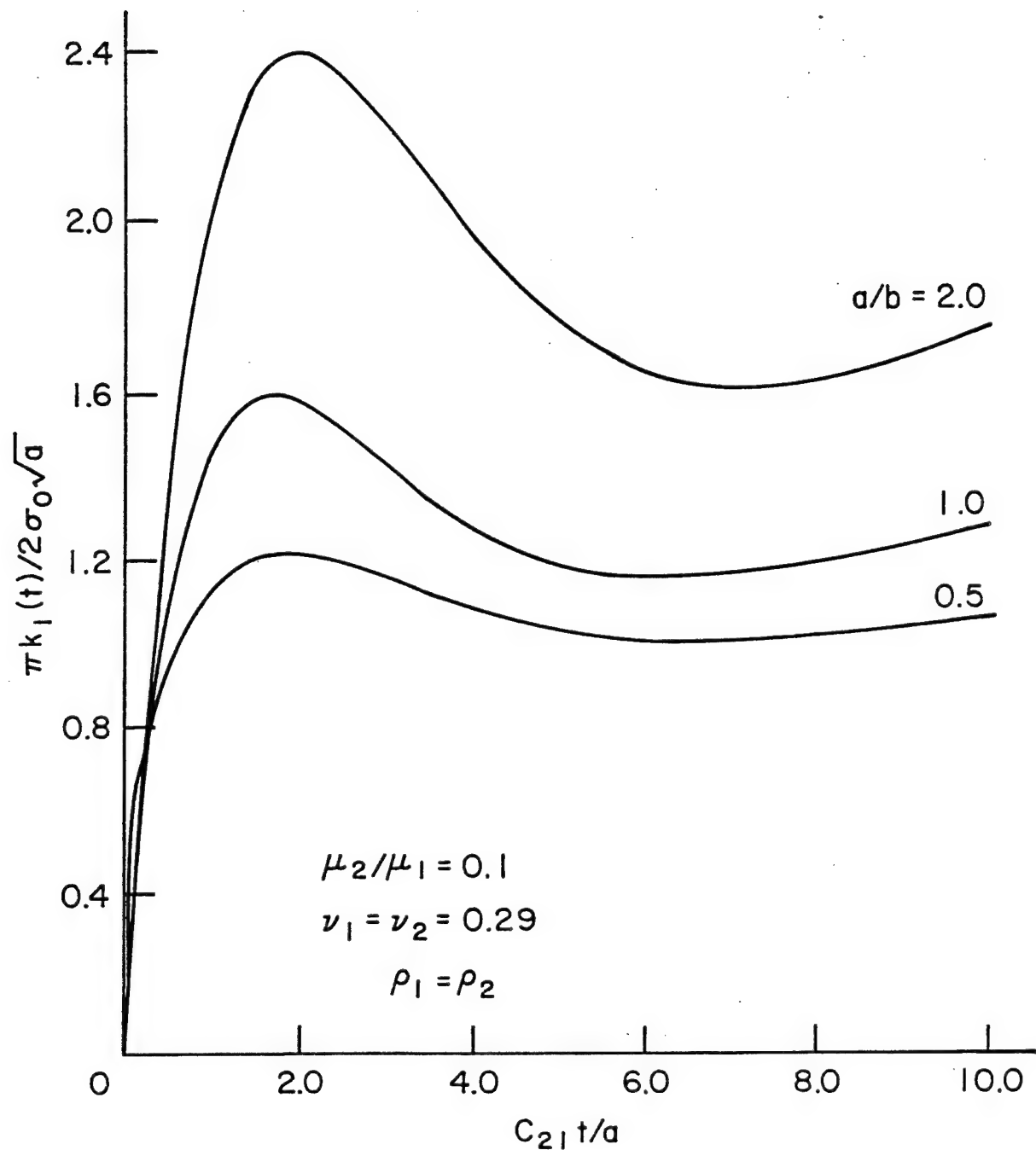


Figure 6 - Dynamic stress intensity factor $k_1(t)$ for penny-shaped crack with $\mu_2/\mu_1 = 0.1$

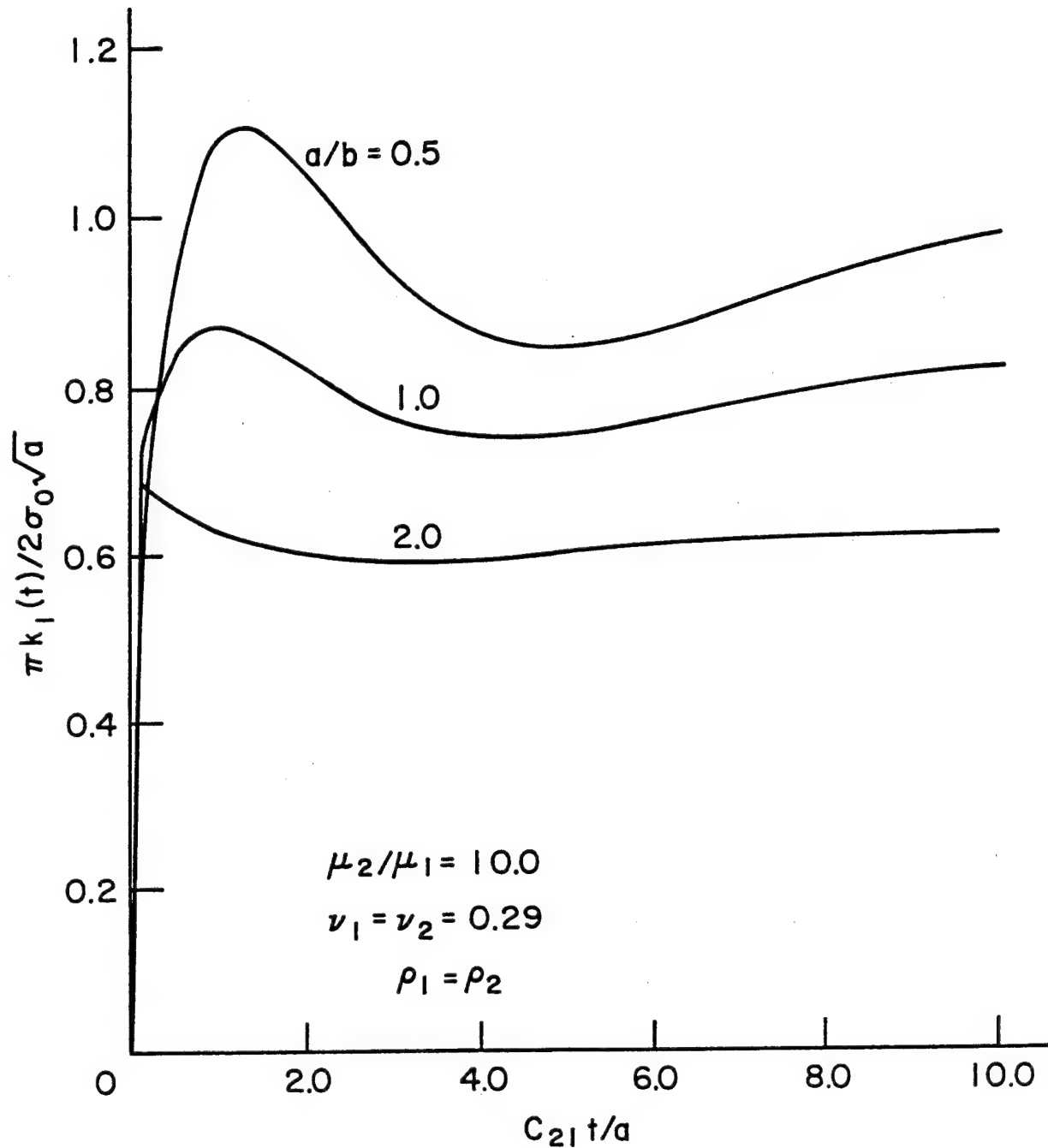


Figure 7 - Dynamic stress intensity factor $k_1(t)$ for penny-shaped crack with $\mu_2/\mu_1 = 10.0$

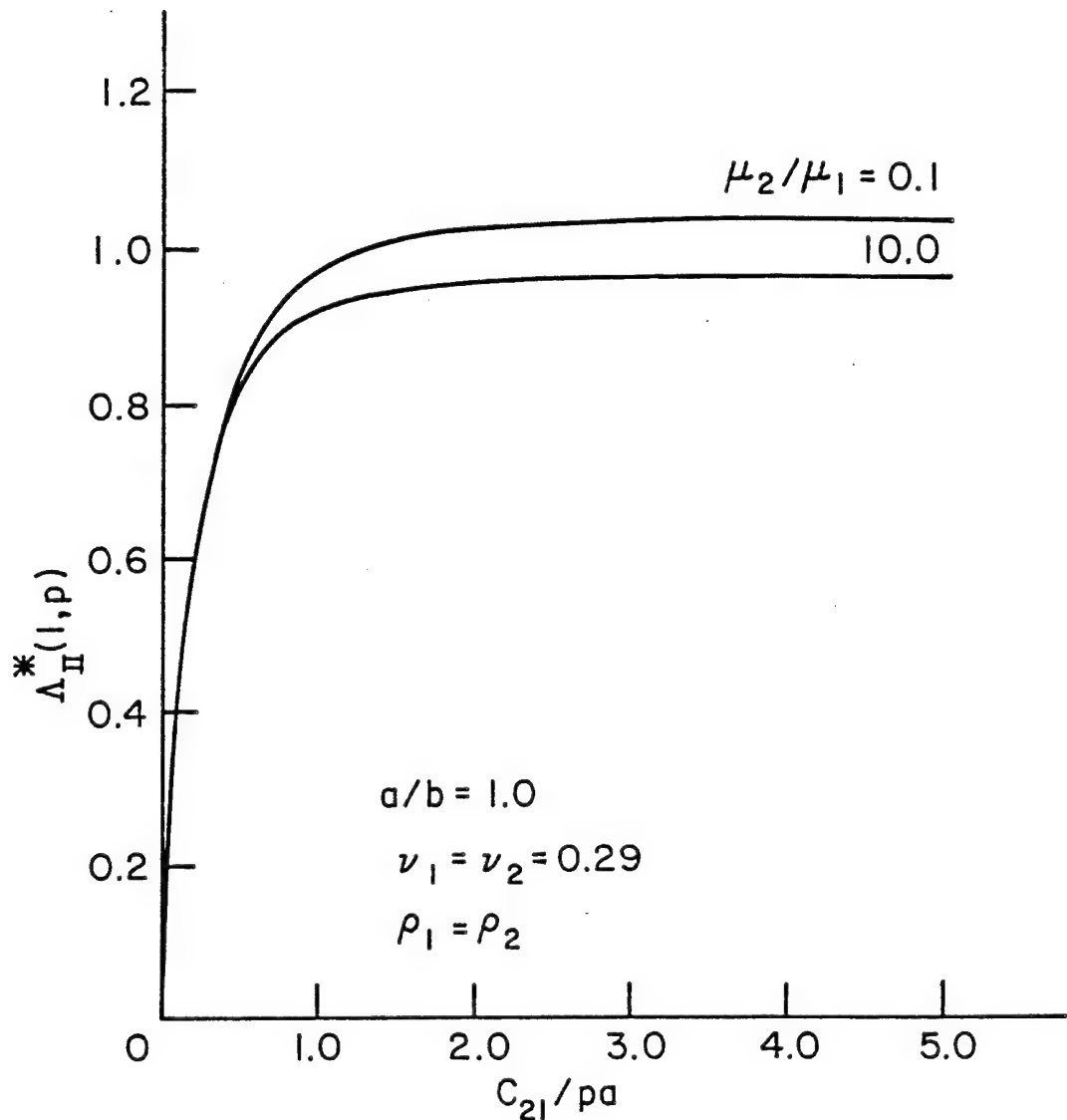


Figure 8 - Variations of $\Lambda_{II}^*(l, p)$ with c_{21}/pa for $a/b = 1.0$

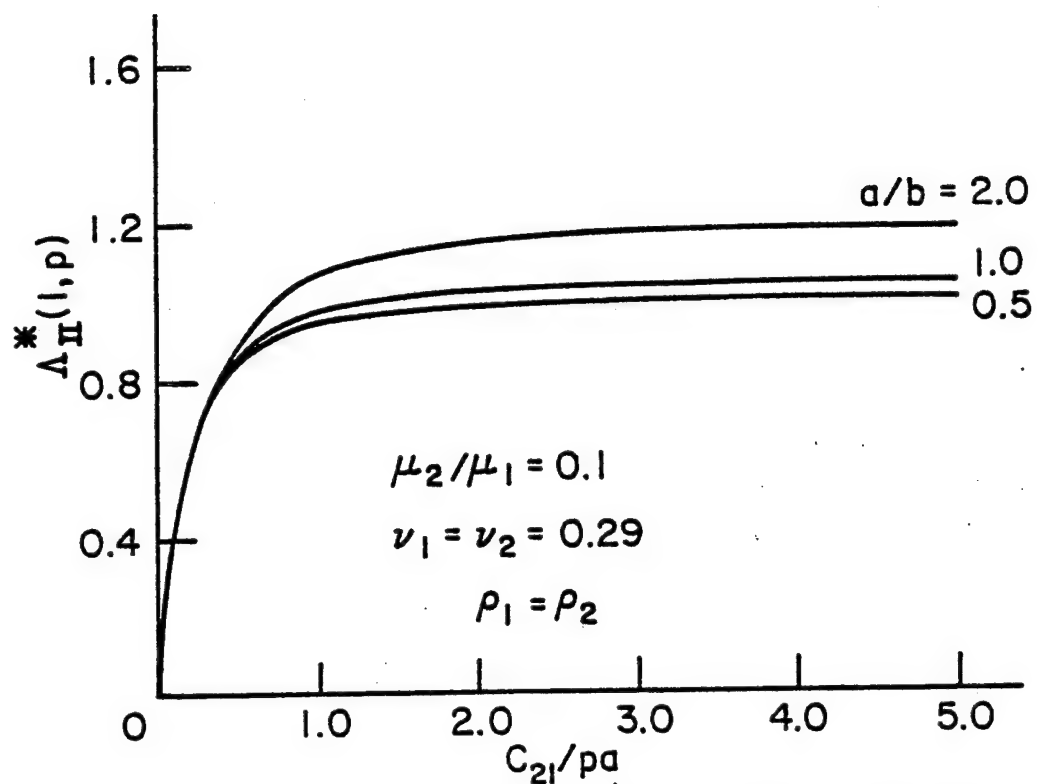


Figure 9 - Variations of $\Lambda_{II}^*(l,p)$ with c_{21}/pa for $\mu_2/\mu_1 = 0.1$ and varying a/b

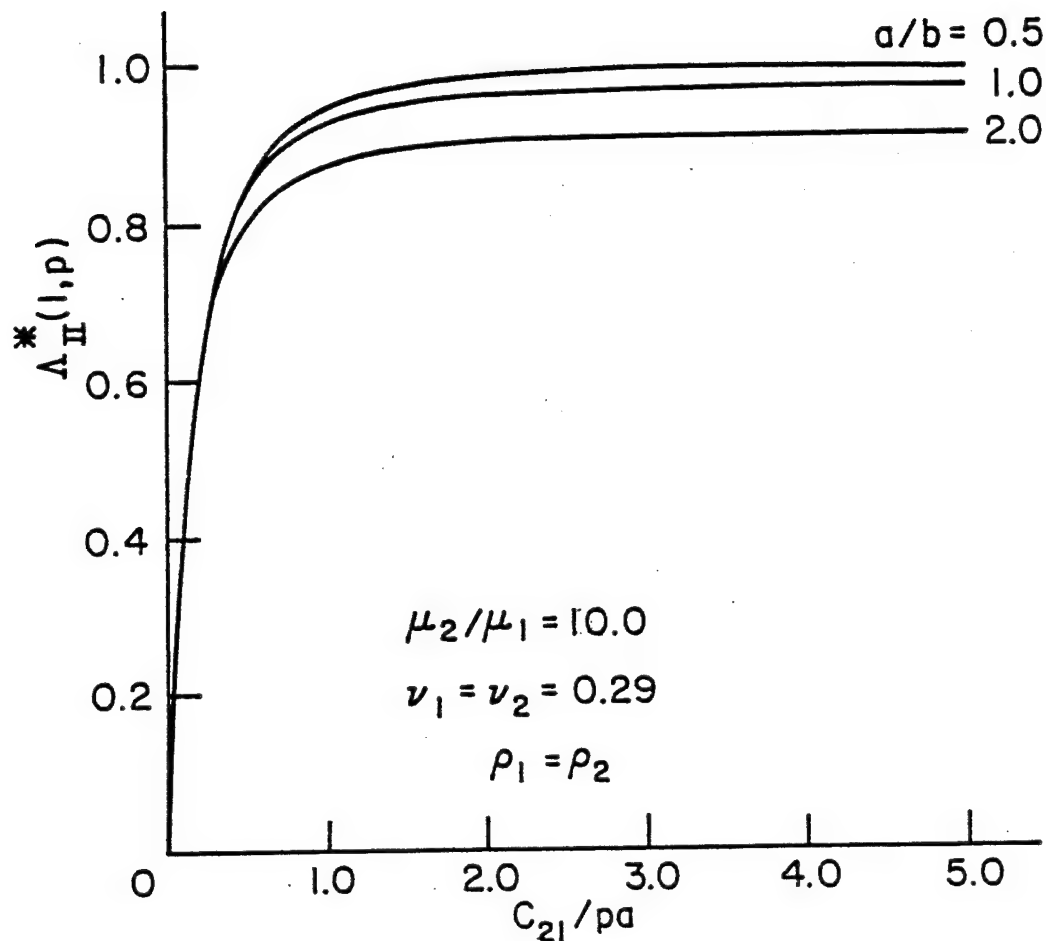


Figure 10 - Variations of $\Lambda_{II}^*(l,p)$ with c_{21}/pa for $\mu_2/\mu_1 = 10$ and varying a/b

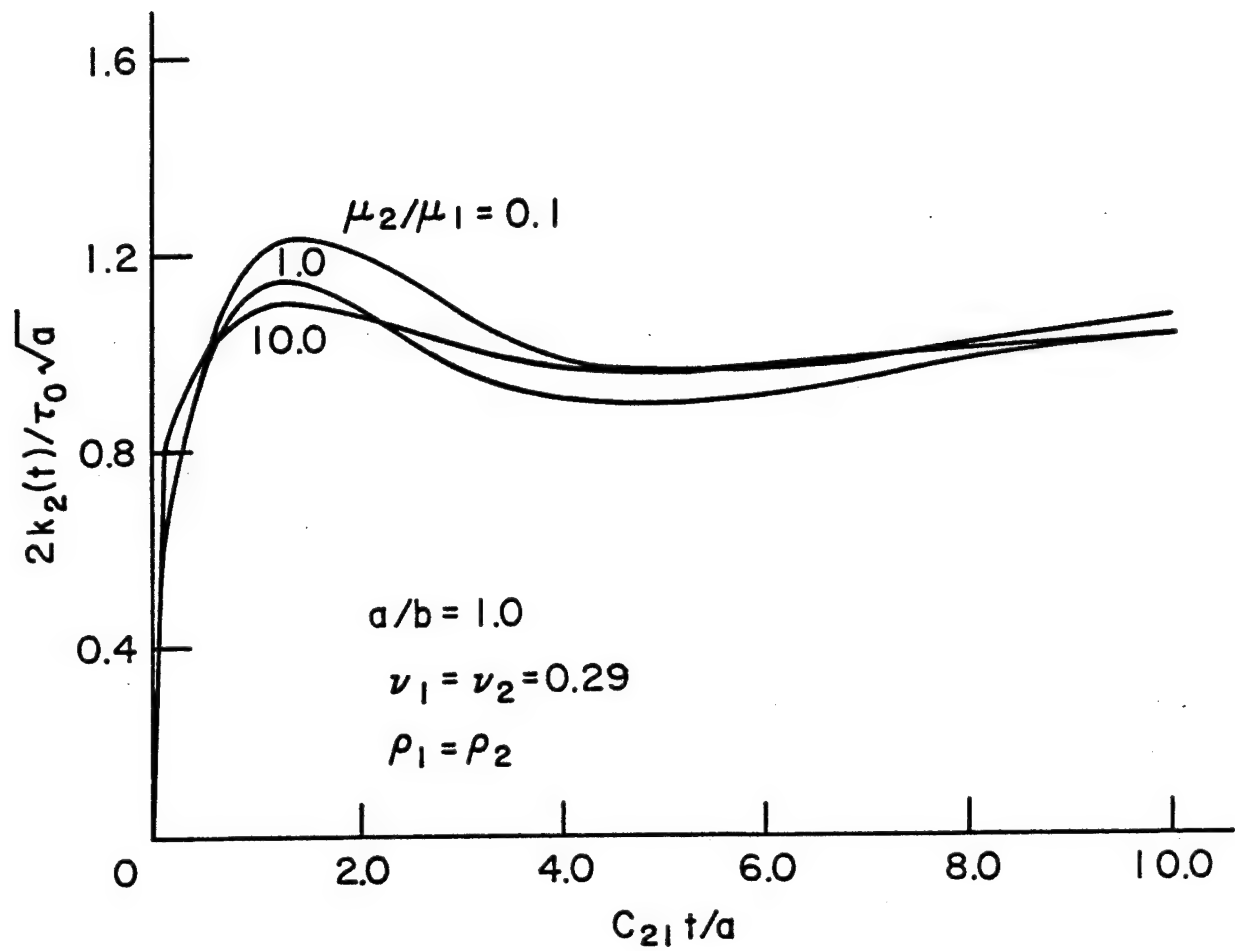


Figure 11 - Stress intensity factor $k_2(t)$ versus time for a penny-shaped crack with $a/b = 1.0$

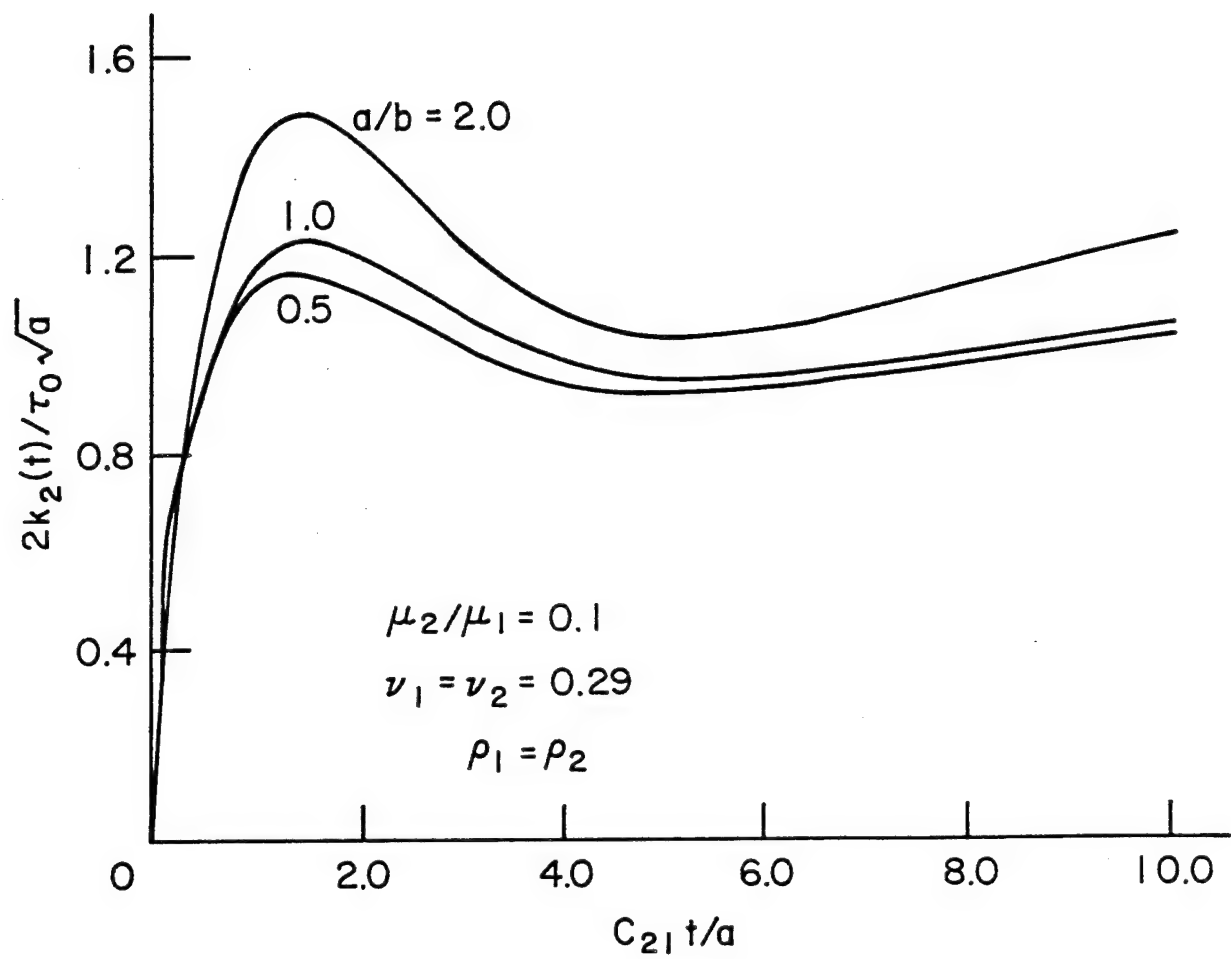


Figure 12 - Stress intensity factor $k_2(t)$ versus time for a penny-shaped crack with $\mu_2/\mu_1 = 0.1$

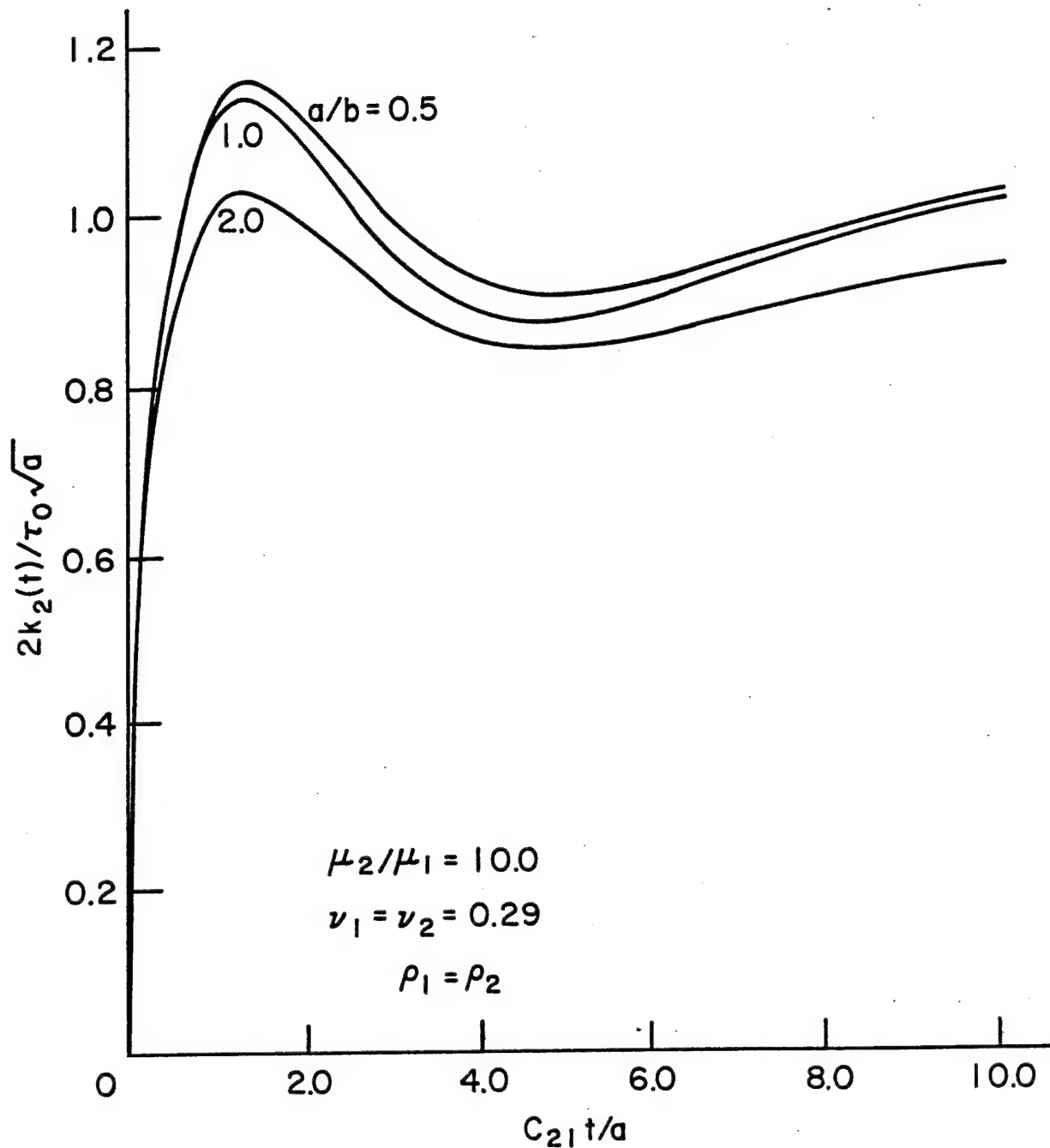


Figure 13 - Stress intensity factor $k_2(t)$ versus time for a penny-shaped crack with $\mu_2/\mu_1 = 10.0$

Axial impact

```

PROGRAM BETA(INPUT,OUTPUT,PUNCH,PLOT,TAPE 99=PLOT)
3  REAL NON(4),F(4,4,1),G(4,4),D(4),PT(4)
3  REAL B(4),C(4)
3  REAL LP(50),DTA(50)
3  EQUIVALENCE (NON,B)
3  COMMON K1,K2,K3,K4
3  COMMON/AUX/H,P,PK1,PK2,BMU,X,Y
3  LP(1)=0.0
3  DTA(1)=0.0
4  READ 2,K1,K2,K3,K4
20  2 FORMAT(I2)
*   K1 = ORDER OF SYSTEM OF EQUATIONS
*   K2 = NO. OF DISTINCT KERNELS
*   K3 = NO. OF DATA POINTS
*   K4 = NO. OF DATA SETS TO BE EVALUATED
*   SET UP DATA POINTS
20  AK=K3
22  DO 5 N=1,K3
23  AN=N
24  5 PT(N)=AN/AK
*   SET UP INTEGRATION MATRIX
31  M=K3-2
33  N=K3-1
34  A=K3
35  A=1.0/(3.*A)
37  DO 10 K=2,M,2
41  10 D(K)=2.*A
46  DO 15 K=1,N,2
47  15 D(K)=4.*A
54  D(K3)=A
*   CALCULATE NONHOMOGENEOUS TERMS
56  RHS=1.0
57  DO 22 I=1,K2
61  PRINT 9
64  9 FORMAT(1H1)
64  READ 61,EMU
72  61 FORMAT(F10.5)
72  DO 999 II=1,K4
74  DO 35 N=1,K3
75  35 NON(N)=RHS*PT(N)
*   CALCULATE KERNEL MATRICES
102 CALL CONST(I)
103 DO 20 N=1,K3
105 DO 20 M=1,K3
106 IF(M-N)25,30,30
111 25 F(M,N,I)=F(N,M,I)
120 GO TO 20
120 30 F(M,N,I)=FU(I,PT(M),PT(N))
131 20 CONTINUE
136 CALL CHANGE(F,G,D,I)
141 CALL LINEQ(G,B,C, K3)
144 DO 40 L=1,K3
146 PRINT 6,PT(L),NON(L)
155 6 FORMAT(5X,F8.4,F15.6)
155 40 CONTINUE
160 LP(II+1)=NON(K3)
162 DTA(II+1)=P
164 999 CONTINUE
166 PUNCH 66,(DTA(IX),LP(IX),IX=1,19)
202 66 FORMAT(2F10.5)
202 CALL LAPINV(DTA,LP)
204 22 CONTINUE
207 END

```

```

6  FUNCTION SIMP(I,A,B)
6  COMMON/AUX/H,P,PK1,PK2,BMU,X,Y
10  DEL=0.25*(B-A)
12  IF(DEL)40,45,50
13  45 SIMP=0.0
14  RETURN
14  50 CONTINUE
14  SA=Z(I,A)+Z(I,B)
14  SB=Z(I,A+2.*DEL)
14  SC=Z(I,A+DEL)+Z(I,A+3.*DEL)
35

```

```

53      S1=(DEL/3.)* (SA+2.*SB+4.*SC)
61      IF (S1.EQ.0.0) GO TO 45
62      K=8
63      35  S3=SB+SC
65      DEL=0.5*DEL
67      SC=Z(I,A+DEL)
75      J=K-1
77      DO 5 N=3,J,2
100     AN=N
101     5   SC=SC+Z(I,A+AN*DEL)
113     S2=(DEL/3.)* (SA+2.*SB+4.*SC)
122     DIF=ABS((S2-S1)/S1)
125     ER=0.01
127     IF (DIF-ER) 30,25,25
131     30  SIMP=S2
133     RETURN
133     25  K=2*K
134     S1=S2
136     IF (K-2048) 35,35,40
140     40  PRINT 42,I,A,B
152     42  FORMAT(5X,* INT. DOES NOT CONVERGE *,I3,2F9.4)
152     PRINT 60,X,Y
162     60  FORMAT(2F10.5)
162     DO 70 J=1,10
166     DIP=J
167     DIP=DIP/10.
171     W=Z(I,DIF)
175     PRINT 60,W
202     70  CONTINUE
206     CALL EXIT
207     END

```

```

7      SUBROUTINE CHANGE(F,G,D,I)
7      REAL F(4,4,1),G(4,4),D(4)
7      COMMON K1,K2,K3,K4
10     DO 10 N=1,K3
11     10  DO 10 M=1,K3
24     G(M,N)=F(M,N,I)*D(N)
30     10  CONTINUE
31     DO 20 N=1,K3
40     20  G(N,N)=G(N,N)+1.0
41     RETURN
END

```

```

7      SUBROUTINE LINEQ(A,B,T,N)
7      REAL A(N,N),B(N),T(N)
10     DO 5 I=2,N
17     5   A(I,1)=A(I,1)/A(1,1)
20     DO 10 K=2,N
22     M=K-1
23     DO 15 I=1,N
23     T(I)=A(I,K)
33     DO 20 J=1,M
34     A(J,K)=T(J)
41     J1=J+1
43     DO 20 I=J1,N
44     T(I)=T(I)-A(I,J)*A(J,K)
55     20  CONTINUE
61     A(K,K)=T(K)
65     IF (K.EQ.N) GO TO 10
66     M=K+1
70     DO 25 I=M,N
71     25  A(I,K)=T(I)/A(K,K)
105    10  CONTINUE
*     BACK SUBSTITUTE
110    DO 30 I=1,N
111    T(I)=B(I)
114    M=I+1
116    IF (M.GT.N) GO TO 30
121    DO 30 J=M,N
122    B(J)=B(J)-A(J,I)*T(I)
132    30  CONTINUE
136    DO 35 I=1,N

```

```

K=N+1-I
B(K)=T(K)/A(K,K)
K1=K-1
IF(K1.EQ.0) GO TO 35
DO 35 J1=1,K1
J=K-J1
T(J)=T(J)-A(J,K)*B(K)
CONTINUE
RETURN
END

```

```

FUNCTION FU(I,A,B)
COMMON/AUX/H,P,PK1,PK2,BMU,X,Y
X=A
Y=B
IF(A*B)5,10,5
10  FU=0.0
      RETURN
      5  SUM=SIMP(I,0.0,5.0)
          ER=0.01
          DEL=5.0
20  UP=DEL+5.0
      ADDL=SIMP(I,DEL,UP)
      DEL=UP
      TEST=ABS(ADDL/SUM)
      SUM=SUM+ADDL
      IF(TEST-ER)15,20,20
15  FU=SQRT(X*Y)*SUM
      RETURN
      END

```

```

SUBROUTINE CONST(I)
COMMON/AUX/H,P,PK1,PK2,BMU,X,Y
PR1=0.29
PR2=0.29
PK1=SQRT((1.-2.*PR1)/(2.*(1.-PR1)))
PK2=SQRT((1.-2.*PR2)/(2.*(1.-PR2)))
READ 1,P
1 FORMAT(F10.5)
HH=0.1
HH=10.0
HH=5.0
HH=4.0
HH=1.0
HH=0.5
HH=2.0
H=1./HH
PRINT 2,BMU,PR1,PR2,HH,F
2 FORMAT(////5X,* MU2/MU1 =*F6.2,* NU1 =*F4.2,* NU2 =*F4.2//5X,* A
1/H =*F4.2,* C21/PA =*F4.2)
RETURN
END

```

```

FUNCTION Z(I,S)
COMMON/AUX/H,P,PK1,PK2,EMU,X,Y
BESJH(A)=SQRT(2.*A/PI)*SIN(A)/A
PI=3.1415926
IF(S-0.0)5,5,10
5 Z=0.0
RETURN
10 CONTINUE
PP=P*P
C1=PK1*PK1
C2=PK2*PK2
CC=1.-C1
GA=SQRT(S*S+C1/PP)
GB=SQRT(S*S+1./PP)
GC=SQRT(S*S+C2/EMU/PP)
GD=SQRT(S*S+1./EMU/PP)
AA=S*S+1./PP/2.
AB=1.-BML

```

```

100
103
110
115
123
131
137
145
152
157
162
164
171
174
200
203
206
211
214
217
222
226
231
233
235
236
240
242
244
246
247
252
256
262
266
275
301
307
312
321
332
337
347
350

AC=S*S-GC*GD
AD=(GB-GD)/AC/PP/2.*BMU
AE=(GB+GD)/AC/PP/2.*BMU
AF=(S*S-GA*GD)/AC/PP/2.*EMU
AG=(S*S+GA*GD)/AC/PP/2.*EMU
AH=(S*S-GB*GC)/AC/PP/2.*BMU
AI=(S*S+GB*GC)/AC/PP/2.*BMU
AJ=(GA-GC)/AC/PP/2.*BMU
AK=(GA+GC)/AC/PP/2.*BMU
A1=-(AB*GB-AD)
A2=AB*GB-AE
A3=AA-BMU*S*S-AF
A4=AA-BMU*S*S-AG
A5=-AA+BMU*S*S+AH
A6=-AA+BMU*S*S+AI
A7=S*(AE*GA-AJ)
A8=-S*(AE*GA-AK)
BA=A1*A6-A2*A5
BB=A3*A6-S*A2*A7
BC=A4*A6-S*A2*A8
BD=S*A1*A7-A3*A5
BE=S*A1*A8-A4*A5
B1=BB/BA
B2=BC/BA
B3=BD/BA
B4=BE/BA
EA=2.*GA*H
EB=2.*GB*H
EC=(EA+EB)/2.
ED=2.*EC
E1=EXP(-EA)
E2=EXP(-EB)
E3=EXP(-EC)
E4=EXP(-ED)
DL=B2+B3*E4+B4*E2+B1*E1
D1=2.*PP/CC/GB/DL
D2=AA*AA-S*S*GA*GB
D3=B2-B3*E4
D4=2.*AA*(GB*(B1*84-B2*B3)-S*S*GA)*E3
D5=(AA*AA+S*S*GA*GB)*(B4*E2-B1*E1)
F=D1*(D2*D3+D4+D5)
Z=(F-S)*EESJH(S*X)*BESJH(S*Y)
RETURN
END

```

SUBROUTINE LAPINV(GLAM, PHI)
 THIS PROGRAM EVALUATES THE COEFFICIENTS FOR SERIES
 OF JACOBI POLYNOMIALS WHICH REPRESENTS A LAPLACE
 INVERSION INTEGRAL

```

REAL MUL
DIMENSION A(50),GLAM(50),PHI(50),C(4,50)
DIMENSION BK(101),TT(101)
COMMON/2/TI,TF,DT,MN,EK,TT
READ 1,NN,MN,MM
1 FORMAT(3I2)
READ 2,JI,TF,DT
2 FORMAT(3F10.5)
PRINT 99
99 FORMAT(1H1)
CALL SPLICE(GLAM,PHI,MM,C)
PRINT 101
101 FORMAT(////5X,* GLAM PHI *)
PRINT 102,(GLAM(I),PHI(I),I=1,MM)
102 FORMAT(5X,F10.5,5X,F10.5)
M11=MM-1
PRINT 300
300 FORMAT(////5X,* C(1,J) C(2,J) C(3,J)
1,J) *)
PRINT 103,((C(I,J),I=1,4),J=1,M11)
103 FORMAT(5X,F10.5,5X,F10.5,5X,F10.5,5X,F10.5)
PRINT 99
DO 10 I=1,NN
READ 3,BET,DEL
3 FORMAT(2F10.5)
PRINT 98,BET,DEL

```

```

140 98 FORMAT(/////5X,*BETA =*F5.3,* DELTA =*F5.3)
140  DO 11 L=1,MN
143  AL=L
144  S=1./(AL+BET)/DEL
150  CALL SPLINE(GLAM,PHI,MM,C,S,G)
153  F=G*S
155  IF(AL-2.)81,82,83
161  81 A(1)=(1.+BET)*DEL*F
165  GO TO 11
165  82 A(2)=((2.+BET)*DEL*F-A(1))*(3.+BET)
175  GO TO 11
175  83 CONTINUE
175  TOP=1.
177  L1=L-1
201  AL1=L1
202  DO 12 J=1,L1
203  AJ=J
204  TOP=AJ*TOP
206  12 CONTINUE
210  L2=2*L-1
212  BOT=1.
214  DO 13 J=L,L2
215  AJ=J
216  BOT=(AJ+BET)*BOT
221  13 CONTINUE
223  MUL=BOT/TOP
225  SUM=0.0
226  DO 14 N=1,L1
227  AN=N
230  IF(AN-2.)85,86,87
233  85 TCD=1.
235  GO TO 88
235  86 TOD=AL1
237  GO TO 88
237  87 CONTINUE
237  TOD=1.
241  ICH=L1-(N-2)
244  DO 15 J=ICH,L1
245  AJ=J
246  TCD=AJ*TCD
250  15 CONTINUE
252  88 CONTINUE
252  BOD=1.
254  JA=L1+N
256  DO 16 J=L,JA
260  AJ=J
261  BOD=BOD*(AJ+BET)
264  16 CONTINUE
266  CO=TOD/BOD
270  SUM=SUM+CO*A(N)
273  14 CONTINUE
275  A(L)=MUL*(DEL*F-SUM)
301  11 CONTINUE
304  CALL JACSER(DEL,A,BET)
306  CALL NAMPLT
307  CALL QIKSET(6.0,0.0,0.0,E.0,0.0,0.0)
313  CALL QIKSAX(3,3)
315  CALL QIKFLT(TT,BK,101)
320  CALL ENDFLT
321  10 CONTINUE
325  999 CONTINUE
325  RETURN
326  END

```

```

6   SUBROUTINE JACSER(D,C,B)
6   DIMENSION C(50),SF(50),P(50)
6   DIMENSION BK(101),TT(101)
6   COMMON/2/TI,TF,DT,MN,BK,TT
6   TT(1)=0.0
7   BK(1)=0.0
7   LM=1
10  T=TI
11
12  T=T+DT
14  X=2.*EXP(-D*T)-1.
24  CALL JACOBI(MN,X,B,P)

```

```

26 SF(1)=C(1)*P(1)
32 DO 10 L=2,MN
33 L1=L-1
35 AL=L
36 SF(L)=SF(L1)+C(L)*P(L)
43 10 CONTINUE
45 PRINT 97,T,X
55 97 FORMAT(////5X,* T =*F6.3,* X =*F10.5)
55 PRINT 96
61 96 FORMAT(///5X,* I C(I) *,5X,* N F(T) *)
61 DO 11 I=1,6
65 PRINT 95,I,C(I),I,SF(I)
95 FORMAT(5X,I2,F10.2,5X,I2,F10.5)
105 11 CONTINUE
105 LM=LM+1
113 BK(LM)=SF(5)
115 TT(LM)=T
117 IF(T.LE.TF) GO TO 12
121 RETURN
122 END

```

```

CC SUBROUTINE JACOBI(N,X,E,PB)
7 THIS PROGRAM CALCULATES JACOBI POLYNOMIALS OF ORDER
7 K-1 WITH ARG X AND PARAMETER B GT -1
10 DIMENSION PB(N)
11 AN=N
12 IF(AN-2.)1,2,3
1  PB(1)=1.
14 RETURN
2 PB(1)=1.
16 PB(2)=X-B*(1.-X)/2.
21 RETURN
3 BSQ=B*B
23 BONE=B+1.
25 PB(1)=1.
26 PB(2)=X-B*(1.-X)/2.
31 DO 4 K=3,N
33 AK=K
34 AK1=AK-1.
36 AK2=AK-2.
40 K1=K-1
42 K2=K-2
43 CO1=((2.*AK1)+B)*X
46 CO1=((2.*AK2)+B)*CO1
51 CO1=((2.*AK2)+BONE)*(CO1-BSQ)
56 CO2=2.*AK2*(AK2+B)*((2.*AK1)+B)
64 CO=2.*AK1*(AK1+B)*((2.*AK2)+B)
71 4 PB(K)=(CO1*PB(K1)-CO2*PB(K2))/CO
102 RETURN
103 END

```

```

11 SUBROUTINE SPLINE(X,Y,M,C,XINT,YINT)
11 DIMENSION X(50),Y(50),C(4,50)
13 IF(XINT-X(1))1,10,11
10 YINT=Y(1)
14 RETURN
11 CONTINUE
15 IF(X(M)-XINT)1,12,13
12 YINT=Y(M)
13 RETURN
14 CONTINUE
15 K=M/2
16 N=M
17 2 CONTINUE
18 IF(X(K)-XINT)3,14,5
19 YINT=Y(K)
20 RETURN
21 3 CONTINUE
22 IF(XINT-X(K+1))4,15,7
23 15 YINT=Y(K+1)
24 RETURN
25 4 CONTINUE
26 YINT=(X(K+1)-XINT)*(C(1,K)+(X(K+1)-XINT)**2+C(3,K))

```

```

YINT=YINT+(XINT-X(K))*C(2,K)*(XINT-X(K))**2+C(4,K))
RETURN
5 CONTINUE
IF(X(K-1)-XINT)6,16,17
6 K=K-1
GO TO 4
16 YINT=Y(K-1)
RETURN
17 N=K
K=K/2
GO TO 2
7 LL=K
K=(N+K)/2
8 CONTINUE
IF(X(K)-XINT)3,14,18
18 CONTINUE
IF(X(K-1)-XINT)6,16,19
19 N=K
K=(LL+K)/2
GO TO 8
1 PRINT 101
101 FORMAT(* OUT OF RANGE FOR INTERPOLATION *)
STOP
ENO

```

```

SUBROUTINE SPLICE(X,Y,M,C)
DIMENSION X(50),Y(50),D(50),P(50),E(50),C(4,50)
DIMENSION A(50,3),B(50),Z(50)
MM=M-1
DO 2 K=1,MM
D(K)=X(K+1)-X(K)
P(K)=D(K)/6.
2 E(K)=(Y(K+1)-Y(K))/D(K)
DO 3 K=2,MM
3 B(K)=E(K)-E(K-1)
A(1,2)=-1.-D(1)/D(2)
A(1,3)=D(1)/D(2)
A(2,3)=P(2)-P(1)*A(1,3)
A(2,2)=2.*(P(1)+P(2))-P(1)*A(1,2)
A(2,3)=A(2,3)/A(2,2)
B(2)=B(2)/A(2,2)
DO 4 K=3,MM
A(K,2)=2.*(P(K-1)+P(K))-P(K-1)*A(K-1,3)
B(K)=B(K)-P(K-1)*B(K-1)
A(K,3)=P(K)/A(K,2)
4 B(K)=B(K)/A(K,2)
Q=D(M-2)/D(M-1)
A(M,1)=1.+Q+A(M-2,3)
A(M,2)=-Q-A(M,1)*A(M-1,3)
B(M)=B(M-2)-A(M,1)*B(M-1)
Z(M)=B(M)/A(M,2)
MN=M-2
DO 6 I=1,MN
K=M-I
6 Z(K)=B(K)-A(K,3)*Z(K+1)
Z(1)=-A(1,2)*Z(2)-A(1,3)*Z(3)
DO 7 K=1,MM
Q=1./((6.*D(K)))
C(1,K)=Z(K)*Q
C(2,K)=Z(K+1)*Q
C(3,K)=Y(K)/D(K)-Z(K)*P(K)
C(4,K)=Y(K+1)/D(K)-Z(K+1)*P(K)
7 RETURN
END

```

Torsional impact

```

PROGRAM BETA(INPUT,OUTPUT,PUNCH,PLOT,TAPE 99=PLOT)
REAL NON(4),F(4,4,1),G(4,4),D(4),PT(4)
REAL B(4),C(4)
REAL LP(50),DTA(50)
EQUIVALENCE (NON,B)
COMMON K1,K2,K3,K4
COMMON/AUX/H,P,PK1,PK2,BMU,X,Y
LP(1)=0.0
DTA(1)=0.0
READ 2,K1,K2,K3,K4
2 FORMAT(I2)
* K1 = ORDER OF SYSTEM OF EQUATIONS
* K2 = NO. OF DISTINCT KERNELS
* K3 = NO. OF DATA POINTS
* K4 = NO. OF DATA SETS TO BE EVALUATED
* SET UP DATA POINTS
AK=K3
DO 5 N=1,K3
A=N
5 PT(N)=AN/AK
* SET UP INTEGRATION MATRIX
M=K3-2
N=K3-1
A=K3
A=1.0/(3.*A)
DO 10 K=2,M,2
10 D(K)=2.*A
DO 15 K=1,N,2
15 D(K)=4.*A
D(K3)=A
* CALCULATE NONHOMOGENEOUS TERMS
RHS=1.0
DO 22 I=1,K2
PRINT 9
9 FORMAT(1H1)
READ 61,BMU
61 FORMAT(F10.5)
DO 999 II=1,K4
999 D(35)=N=1,K3
35 NON(N)=RHS*PT(N)*PT(N)
* CALCULATE KERNEL MATRICES
CALL CONST(I)
DO 20 N=1,K3
DO 20 M=1,K3
IF(M-N)25,30,30
25 F(M,N,I)=F(N,M,I)
GOTO 20
30 F(M,N,I)=FU(I,PT(M),PT(N))
20 CONTINUE
CALL CHANGE(F,G,D,I)
CALL LINEQ(G,B,C,K3)
DO 40 L=1,K3
PRINT 6,PT(L),NON(L)
40 FORMAT(5X,F8.4,F15.6)
CONTINUE
LP(II+1)=NON(K3)
DTA(II+1)=P
999 CONTINUE
PUNCH 66,(DTA(IX),LP(IX),IX=1,19)
66 FORMAT(2F10.5)
CALL LAPINV(DTA,LP)
22 CONTINUE
END

```

```

FUNCTION SIMP(I,A,B)
COMMON/AUX/H,P,PK1,PK2,BMU,X,Y
DEL=0.25*(B-A)
IF(DEL)40,45,50
45 SIMP=0.0
RETURN
50 CONTINUE
SA=Z(I,A)+Z(I,B)
SB=Z(I,A+2.*DEL)
SC=Z(I,A+DEL)+Z(I,A+3.*DEL)

```

```

53      S1=(DEL/3.)*(SA+2.*SB+4.*SC)
51      IF(S1.EQ.0.0) GO TO 45
52      K=8
53      35  SB=SB+SC
54      DEL=0.5*DEL
55      SC=Z(I,A+DEL)
56      J=K-1
57      DO 5 N=3,J,2
58      AN=N
59      5   S C=SC+Z(I,A+AN*DEL)
60      S2=(DEL/3.)*(SA+2.*SB+4.*SC)
61      DIF=ABS((S2-S1)/S1)
62      ER=0.01
63      IF(DIF-ER)30,25,25
64      30  SIMP=S2
65      RETURN
66      25  K=2*K
67      S1=S2
68      IF(K-2048)35,35,40
69      40  PRINT 42,I,A,B
70      42  FORMAT(5X,* INT. DOES NOT CONVERGE *,I3,2F9.4)
71      PRINT 60,X,Y
72      60  FORMAT(2F10.5)
73      DO 70 J=1,10
74      DIP=J
75      DIP=DIP/10.
76      W=Z(I,DIP)
77      PRINT 60,W
78      70  CONTINUE
79      CALL EXIT
80      END

```

```

SUBROUTINE CHANGE(F,G,D,I)
REAL F(4,4,1),G(4,4),D(4)
COMMON K1,K2,K3,K4
DO 10 N=1,K3
DC 10 M=1,K3
G(M,N)=F(M,N,I)*D(N)
10  CONTINUE
DO 20 N=1,K3
20  G(N,N)=G(N,N)+1.0
RETURN
END

```

```

SUBROUTINE LINEQ(A,B,T,N)
REAL A(N,N),B(N),T(N)
DO 5 I=2,N

```

```

5   A(I,1)=A(I,1)/A(1,1)
DO 10 K=2,N
M=K-1
DO 15 I=1,N
15  T(I)=A(I,K)
DC 20 J=1,M
A(J,K)=T(J)
J1=J+1
DC 20 I=J1,N
T(I)=T(I)-A(I,J)*A(J,K)
20  CONTINUE
A(K,K)=T(K)
IF(K.EQ.N) GO TO 10
M=K+1
DO 25 I=M,N
25  A(I,K)=T(I)/A(K,K)
10  CONTINUE

```

```

* BACK SUBSTITUTE
DO 30 I=1,N
T(I)=B(I)
M=I+1
IF(M.GT.N) GO TO 30
DO 30 J=M,N
B(J)=B(J)-A(J,I)*T(I)
30  CONTINUE
DO 35 I=1,N

```

```

      K=N+1-I
      B(K)=T(K)/A(K,K)
      K1=K-1
      IF(K1.EQ.0) GO TO 35
      DO 35 J1=1,K1
      J=K-J1
      T(J)=T(J)-A(J,K)*B(K)
      CONTINUE
      RETURN
      END
  35

```

```

FUNCTION FU(I,A,B)
COMMON/AUX/H,P,PK1,PK2,BMU,X,Y
X=A
Y=B
IF(A*B)5,10,5
10 FU=0.0
      RETURN
      5 SUM=SIMP(I,0.0,5.0)
      ER=0.01
      DEL =5.0
20 UP=DEL+5.0
      ADDL=SIMP(I,DEL,UP)
      DEL =UP
      TEST=ABS(ADDL/SUM)
      SUM=SUM+ADDL
      IF(TEST-ER)15,20,20
15 FU=SQRT(X*Y)*SUM
      RETURN
      END

```

```

SUBROUTINE CONST(I)
COMMON/AUX/H,P,PK1,PK2,BMU,X,Y
PR1=0.29
PR2=0.29
PK1=SQRT((1.-2.*PR1)/(2.*(1.-PR1)))
PK2=SQRT((1.-2.*PR2)/(2.*(1.-PR2)))
READ 1,P
1 FORMAT(F10.5)
H T=5.0
HH=0.2
HH=0.5
HH=1.0
HH=2.0
H=1./HH
PRINT 2,BMU,PR1,PR2,HH,P
2 FORMAT(//5X,* MU2/MU1 =*F6.2,* NU1 =*F4.2,* NU2 =*F4.2//5X,* A
1/H =*F4.2,* C21/PA =*F4.2)
RETURN
END

```

```

FUNCTION Z(I,S)
COMMON/AUX/H,P,PK1,PK2,BMU,X,Y
BESJT(A)=SQRT(2.*A/PI)*(SIN(A)/A/A-COS(A)/A)
PI=3.1415926
IF (S-0.0)5,5,10
5 Z=0.0
RETURN
10 CNTINUE
PP=P*P
GB=SQRT(S*S+1./PP)
GD=SQRT(S*S+1./BMU/PP)
AA=1.-BMU*GD/GB
AB=1.+BMU*GD/GB
AC=1.-AA/AB*EXP(-2.*GB*H)
AD=1.+AA/AB*EXP(-2.*GB*H)
F=GB*AC/AD
Z=(F-S)*BESJT(S*X)*BESJT(S*Y)
RETURN
END

```

```

C SUBROUTINE LAPINV(GLAM,PHI)
C THIS PROGRAM EVALUATES THE COEFFICIENTS FOR SERIES
C OF JACOBI POLYNOMIALS WHICH REPRESENTS A LAPLACE
C INVERSION INTEGRAL
C REAL MUL
C DIMENSION A(50),GLAM(50),PHI(50),C(4,50)
C DIMENSION BK(101),TT(101)
C COMMON/2/TI,TF,DT,MN,BK,TT
C READ 1,NN,MN,MM
1 16 FORMAT(3I2)
16 20 READ 2,TI,TF,DT
20 24 FORMAT(3F10.5)
24 28 PRINT 99
28 32 99 FORMAT(1H1)
32 36 CALL SPLICE(GLAM,PHI,MM,C)
36 40 PRINT 101
40 44 FORMAT(////5X,* GLAM PHI *)
44 48 PRINT 102,(GLAM(I),PHI(I),I=1,MM)
48 52 102 FORMAT(5X,F10.5,5X,F10.5)
52 56 M11=MM-1
56 60 PRINT 300
60 64 300 FORMAT(////5X,* C(1,J) C(2,J) C(3,J) C(4
64 68 1,J) *)
68 72 PRINT 103,((C(I,J),I=1,4),J=1,M11)
72 76 103 FORMAT(5X,F10.5,5X,F10.5,5X,F10.5,5X,F10.5)
76 80 PRINT 99
80 84 DO 10 I=1,NN
84 88 READ 3,BET,DEL
88 92 3 FORMAT(2F10.5)
92 96 PRINT 98,BET,DEL
96 100 98 FORMAT(////5X,*BETA =*F5.3,* DELTA =*F5.3)
100 104 DO 11 L=1,MN
104 108 AL=L
108 112 S=1./(AL+BET)/DEL
112 116 CALL SPLINE(GLAM,PHI,MM,C,S,G)
116 120 F=G*S
120 124 IF(AL-2.)81,82,83
81 128 A(1)=(1.+BET)*DEL*F
82 132 GO TO 11
82 136 A(2)=((2.+BET)*DEL*F-A(1))*(3.+BET)
82 140 GO TO 11
83 144 CONTINUE
83 148 TOP=1.
83 152 L1=L-1
83 156 AL1=L1
83 160 DO 12 J=1,L1
83 164 AJ=J
83 168 TOP=AJ*TOP
83 172 12 CONTINUE
83 176 L2=2*L-1
83 180 BOT=1.
83 184 DO 13 J=L,L2
83 188 AJ=J
83 192 BOT=(AJ+BET)*BOT
83 196 13 CONTINUE
83 200 MUL=BOT/TOP
83 204 SUM=0.0
83 208 DO 14 N=1,L1
83 212 AN=N
83 216 IF(AN-2.)85,86,87
85 220 TOD=1.
85 224 GO TO 88
86 228 TOD=AL1
86 232 GO TO 88
87 236 CONTINUE
87 240 TOD=1.
87 244 ICH=L1-(N-2)
87 248 DO 15 J=ICH,L1
87 252 AJ=J
87 256 TOD=AJ*TOD
87 260 15 CONTINUE
88 264 CONTINUE
88 268 BOD=1.
88 272 JA=L1+N
88 276 DO 16 J=L,JA
88 280 AJ=J

```

```

2 E1      BOD=BOD*(AJ+BET)
2 E4      16  CONTINUE
266      CO=TOD/BOD
270      SUM=SUM+CO*A(N)
273      14  CONTINUE
275      A(L)=MUL*(DEL*F-SUM)
301      11  CONTINUE
304      CALL JACSER(DEL,A,BET)
306      CALL NAMPLT
307      CALL QIKSET(6.0,0.0,0.0,6.0,0.0,0.0)
313      CALL QIKSAX(3,3)
315      CALL QIKPLT(TT,BK,101)
320      CALL ENDPLT
321      10  CONTINUE
325      999 CONTINUE
325      RETURN
326      END

```

```

6      SUBROUTINE JACSER(D,C,B)
6      DIMENSION C(50),SF(50),P(50)
6      DIMENSION BK(101),TT(101)
6      COMMON/2/TI,TF,DT,MN,BK,TT
6      TT(1)=0.0
6      BK(1)=0.0
10     LM=1
11     T=TI
12     T=T+DT
14     X=2.*EXP(-D*T)-1.
24     CALL JACOBI(MN,X,B,P)
26     SF(1)=C(1)*P(1)
32     DO 10 L=2,MN
33     L1=L-1
35     AL=L
36     SF(L)=SF(L1)+C(L)*P(L)
43     10  CONTINUE
45     PRINT 97,T,X
55     97  FORMAT(//5X,* T =*F6.3,* X =*F10.5)
55     PRINT 96
61     96  FORMAT(//5X,* I C(I) *,5X,* N F(T) *)
61     DO 11 I=1,6
65     PRINT 95,I,C(I),I,SF(I)
95     FORMAT(5X,I2,F10.2,5X,I2,F10.5)
105    11  CONTINUE
105    LM=LM+1
113    BK(LM)=SF(5)
115    TT(LM)=T
117    IF(T.LE.TF) GO TO 12
121    RETURN
122    END

```

```

C      SUBROUTINE JACOBI(N,X,B,PB)
C      THIS PROGRAM CALCULATES JACOBI POLYNOMIALS OF ORDER
C      K-1 WITH ARG X AND PARAMETER B GT -1
C      DIMENSION PB(N)
7      AN=N
7      1 F(AN-2)=1,2,3
10     1 PB(1)=1.
12     RETURN
14     2 PB(1)=1.
16     PB(2)=X-B*(1.-X)/2.
18     RETURN
20     3 BSQ=B*B
22     BONE=B+1.
24     PB(1)=1.
26     PB(2)=X-B*(1.-X)/2.
28     DO 4 K=3,N
30     AK=K
32     AK1=AK-1.
34     AK2=AK-2.
36     K1=K-1
38     K2=K-2
40     C01=((2.*AK1)+B)*X
42     C01=((2.*AK2)+B)*C01

```

```

51      C01=(2.*AK2)+BONE)*(C01-BSQ)
56      C02=2.*AK2*(AK2+B)*(2.*AK1)+B)
64      C0=2.*AK1*(AK1+B)*(2.*AK2)+B)
71      4 PB(K)=(C01*PB(K1)-C02*PB(K2))/C0
1 02      RETURN
1 03      END

11      SUBROUTINE SPLINE(X,Y,M,C,XINT,YINT)
11      DIMENSION X(50),Y(50),C(4,50)
13      IF(XINT-X(1))1,10,11
10      10 YINT=Y(1)
11      RETURN
12      11 CONTINUE
13      IF(X(M)-XINT)1,12,13
12      12 YINT=Y(M)
13      RETURN
13      13 CONTINUE
14      K=M/2
15      N=M
16      2 CONTINUE
17      IF(X(K)-XINT)3,14,5
14      14 YINT=Y(K)
15      RETURN
16      3 CONTINUE
17      IF(XINT-X(K+1))4,15,7
15      15 YINT=Y(K+1)
16      RETURN
17      4 CONTINUE
18      YINT=(X(K+1)-XINT)*(C(1,K)*(X(K+1)-XINT)**2+C(3,K))
19      YINT=YINT+(XINT-X(K))*(C(2,K)*(XINT-X(K)**2+C(4,K))
20      RETURN
21      5 CONTINUE
22      IF(X(K-1)-XINT)6,16,17
23      6 K=K-1
24      GO TO 4
25      16 YINT=Y(K-1)
26      RETURN
27      17 N=K
28      K=K/2
29      GC TO 2
30      7 LL=K
31      K=(N+K)/2
32      8 CONTINUE
33      IF(X(K)-XINT)3,14,18
34      18 CONTINUE
35      IF(X(K-1)-XINT)6,16,19
36      19 N=K
37      K=(LL+K)/2
38      GC TO 8
39      1 PRINT 101
40      101 FORMAT(* OUT OF RANGE FOR INTERPOLATION *)
41      STOP
42      END

```

```

7      SUBROUTINE SPLICE(X,Y,M,C)
7      DIMENSION X(50),Y(50),D(50),P(50),E(50),C(4,50)
7      DIMENSION A(50,3),B(50),Z(50)
11      MM=M-1
12      DO 2 K=1,MM
13      D(K)=X(K+1)-X(K)
14      P(K)=D(K)/6.
15      2 E(K)=(Y(K+1)-Y(K))/D(K)
16      DO 3 K=2,MM
17      3 B(K)=E(K)-E(K-1)
18      A(1,2)=-1.-D(1)/D(2)
19      A(1,3)=D(1)/D(2)
20      A(2,3)=P(2)-P(1)*A(1,3)
21      A(2,2)=2.*(P(1)+P(2))-P(1)*A(1,2)
22      A(2,3)=A(2,3)/A(2,2)
23      B(2)=B(2)/A(2,2)
24      DO 4 K=3,MM
25      A(K,2)=2.*(P(K-1)+P(K))-P(K-1)*A(K-1,3)
26      B(K)=B(K)-P(K-1)*B(K-1)

```

```

65      A(K,3)=P(K)/A(K,2)
70      B(K)=B(K)/A(K,2)
74      Q=D(M-2)/D(M-1)
76      A(M,1)=1.+Q+A(M-2,3)
101     A(M,2)=-Q-A(M,1)*A(M-1,3)
105     B(M)=B(M-2)-A(M,1)*B(M-1)
112     Z(M)=B(M)/A(M,2)
114     MN=M-2
116     DO 6 I=1,MN
117     K=M-I
120     6 Z(K)=B(K)-A(K,3)*Z(K+1)
127     Z(1)=-A(1,2)*Z(2)-A(1,3)*Z(3)
133     DO 7 K=1,MM
135     Q=1./ (6.*D(K))
140     C(1,K)=Z(K)*Q
143     C(2,K)=Z(K+1)*Q
146     C(3,K)=Y(K)/D(K)-Z(K)*P(K)
154     C(4,K)=Y(K+1)/D(K)-Z(K+1)*P(K)
165     RETURN
165     ENO

```

INTERIM REPORT DISTRIBUTION LIST

NSG 3179

"NORMAL AND RADIAL IMPACT OF COMPOSITES WITH EMBEDDED
PENNY-SHAPED CRACKS"

Advanced Research Projects Agency
Washington DC 20525
Attn: Library

Advanced Technology Center, Inc.
LTV Aerospace Corporation
P.O. Box 6144
Dallas, TX 75222
Attn: D. H. Petersen
W. J. Renton

Air Force Flight Dynamics Laboratory
Wright-Patterson Air Force Base, OH 45433
Attn: L. J. Obery (TBP)
G. P. Sendeckyj (FBC)
R. S. Sandhu

Air Force Materials Laboratory
Wright-Patterson Air Force Base, OH 45433
Attn: H. S. Schwartz (LN)
T. J. Reinhart (MBC)
G. P. Peterson (LC)
E. J. Morrisey (LAE)
S. W. Tsai (MBM)
N. J. Pagano
J. M. Whitney (MBM)

Air Force Office of Scientific Research
Washington DC 20333
Attn: J. F. Masi (SREP)

Air Force Office of Scientific Research
1400 Wilson Blvd.
Arlington, VA 22209

AFOSR/NA
Bolling AFB, DC 20332
Attn: W. J. Walker

Air Force Rocket Propulsion Laboratory
Edwards, CA 93523
Attn: Library

Babcock & Wilcox Company
Advanced Composites Department
P.O. Box 419
Alliance, Ohio 44601
Attn: P. M. Leopold

Bell Helicopter Company
P.O. Box 482
Ft. Worth, TX 76101
Attn: H. Zinberg

The Boeing Company
P. O. Box 3999
Seattle, WA 98124
Attn: J. T. Hoggatt, MS. 88-33
T. R. Porter

The Boeing Company
Vertol Division
Morton, PA 19070
Attn: R. A. Pinckney
E. C. Durchlaub

Battelle Memorial Institute
Columbus Laboratories
505 King Avenue
Columbus, OH 43201
Attn: E. F. Rybicki
L. E. Hulbert

Brunswick Corporation
Defense Products Division
P. O. Box 4594
43000 Industrial Avenue
Lincoln, NE 68504
Attn: R. Morse

Celanese Research Company
86 Morris Ave.
Summit, NJ 07901
Attn: H. S. Klinger

Chemical Propulsion Information Agency
Applied Physics Laboratory
8621 Georgia Avenue
Silver Spring, MD 20910
Attn: Library

Commander
Natick Laboratories
U. S. Army
Natick, MA 01762
Attn: Library

Commander
Naval Air Systems Command
U. S. Navy Department
Washington DC 20360
Attn: M. Stander, AIR-43032D

Commander
Naval Ordnance Systems Command
U.S. Navy Department
Washington DC 20360
Attn: B. Drimmer, ORD-033
M. Kinna, ORD-033A

Cornell University
Dept. Theoretical & Applied Mech.
Thurston Hall
Ithaca, NY 14853
Attn: S. L. Phoenix

Defense Metals Information Center
Battelle Memorial Institute
Columbus Laboratories
505 King Avenue
Columbus, OH 43201

Department of the Army
U.S. Army Material Command
Washington DC 20315
Attn: AMCRD-RC

Department of the Army
U.S. Army Aviation Materials Laboratory
Ft. Eustis, VA 23604
Attn: I. E. Figge, Sr.
Library

Department of the Army
U.S. Army Aviation Systems Command
P.O. Box 209
St. Louis, MO 63166
Attn: R. Vollmer, AMSAV-A-UE

Department of the Army
Plastics Technical Evaluation Center
Picatinny Arsenal
Dover, NJ 07801
Attn: H. E. Pebly, Jr.

Department of the Army
Watervliet Arsenal
Watervliet, NY 12189
Attn: G. D'Andrea

Department of the Army
Watertown Arsenal
Watertown, MA 02172
Attn: A. Thomas

Department of the Army
Redstone Arsenal
Huntsville, AL 35809
Attn: R. J. Thompson, AMSMI-RSS

Department of the Navy
Naval Ordnance Laboratory
White Oak
Silver Spring, MD 20910
Attn: R. Simon

Department of the Navy
U.S. Naval Ship R&D Laboratory
Annapolis, MD 21402
Attn: C. Hersner, Code 2724

Director
Deep Submergence Systems Project
6900 Wisconsin Avenue
Washington DC 20015
Attn: H. Bernstein, DSSP-221

Director
Naval Research Laboratory
Washington DC 20390
Attn: Code 8430
I. Wolock, Code 8433

Drexel University
32nd and Chestnut Streets
Philadelphia, PA 19104
Attn: P. C. Chou

E. I. DuPont DeNemours & Co.
DuPont Experimental Station
Wilmington, DE 19898
Attn: C. H. Zweben

Fiber Science, Inc.
245 East 157 Street
Gardena, CA 90248
Attn: E. Dunahoo

General Dynamics
P.O. Box 748
Ft. Worth, TX 76100
Attn: M. E. Waddoups
Library

General Dynamics/Convair
P.O. Box 1128
San Diego, CA 92112
Attn: J. L. Christian

General Electric Co.
Ervendale, OH 45215
Attn: C. Stotler
R. Ravenhall
R. Stabrylla

General Motors Corporation
Detroit Diesel-Allison Division
Indianapolis, IN 46244
Attn: M. Herman

Georgia Institute of Technology
School of Aerospace Engineering
Atlanta, GA 30332
Attn: L. W. Rehfield

Grumman Aerospace Corporation
Bethpage, Long Island, NY 11714
Attn: S. Dastin
J. B. Whiteside

Hamilton Standard Division
United Aircraft Corporation
Windsor Locks, CT 06096
Attn: W. A. Percival

Hercules, Inc.
Allegheny Ballistics Laboratory
P. O. Box 210
Cumberland, MD 21053
Attn: A. A. Vicario

Hughes Aircraft Company
Culver City, CA 90230
Attn: A. Knoell

Illinois Institute of Technology
10 West 32 Street
Chicago, IL 60616
Attn: L. J. Broutman

IIT Research Institute
10 West 35 Street
Chicago, IL 60616
Attn: I. M Daniel

Jet Propulsion Laboratory
4800 Oak Grove Drive
Pasadena, CA 91103
Attn: Library

Lawrence Livermore Laboratory
P.O. Box 808, L-421
Livermore, CA 94550
Attn: T. T. Chiao
E. M. Wu

Lehigh University
Institute of Fracture &
Solid Mechanics
Bethlehem, PA 18015
Attn: G. C. Sih

Lockheed-Georgia Co.
Advanced Composites Information Center
Dept. 72-14, Zone 402
Marietta, GA 30060
Attn: T. M. Hsu

Lockheed Missiles and Space Co.
P.O. Box 504
Sunnyvale, CA 94087
Attn: R. W. Fenn

Lockheed-California
Burbank, CA 91503
Attn: J. T. Ryder
K. N. Lauraitis
J. C. Ekwall

McDonnell Douglas Aircraft Corporation
P.O. Box 516
Lambert Field, MS 63166
Attn: J. C. Watson

McDonnell Douglas Aircraft Corporation
3855 Lakewood Blvd.
Long Beach, CA 90810
Attn: L. B. Greszczuk

Material Sciences Corporation
1777 Walton Road
Blue Bell, PA 19422
Attn: B. W. Rosen

Massachusetts Institute of Technology
Cambridge, MA 02139
Attn: F. J. McGarry
J. F. Mandell
J. W. Mar

NASA-Ames Research Center
Moffett Field, CA 94035
Attn: Library

NASA-Flight Research Center
P.O. Box 273
Edwards, CA 93523
Attn: Library

NASA-George C. Marshall Space Flight Center
Huntsville, AL 35812
Attn: C. E. Cataldo, S&E-ASTN-MX
Library

NASA-Goddard Space Flight Center
Greenbelt, MD 20771
Attn: Library

NASA-Langley Research Center
Hampton, VA 23365
Attn: E. E. Mathauser, MS 188a
R. A. Pride, MS 188a
M. C. Card
J. R. Davidson

NASA-Lewis Research Center
21000 Brookpark Road
Cleveland, Ohio 44135
Attn: Administration & Technical Service Section
Tech. Report Control, MS. 5-5
Tech. Utilization, MS 3-19
AFSC Liaison, MS. 501-3
Rel. and Quality Assur., MS 500-211
C. P. Blankenship, MS 105-1
R. F. Lark, MS 49-3
J. C. Freche, MS 49-1
R. H. Johns, MS 49-3
C. C. Chamis, MS 49-3 (17 copies)
T. T. Serafini, MS 49-1
Library, MS 60-3 (2 copies)

NASA-Lyndon B. Johnson Space Center
Houston, TX 77001
Attn: S. Glorioso, SMD-ES52
Library

NASA Scientific and Tech. Information Facility
P.O. Box 8757
Balt/Wash International Airport, MD 21240
Attn: Acquisitions Branch (10 copies)

National Aeronautics & Space Administration
Office of Advanced Research & Technology
Washington DC 20546
Attn: M. J. Salkind, Code RWS
D. P. Williams, Code RWS

National Aeronautics & Space Administration
Office of Technology Utilization
Washington DC 20546

National Bureau of Standards
Eng. Mech. Section
Washington DC 20234
Attn: R. Mitchell

National Technology Information Service
Springfield, VA 22151 (6 copies)

National Science Foundation
Engineering Division
1800 G. Street, NW
Washington DC 20540
Attn: Library

Northrop Corporation Aircraft Group
3901 West Broadway
Hawthorne, CA 90250
Attn: R. M. Verette
G. C. Grimes

Pratt & Whitney Aircraft
East Hartford, CT 06108
Attn: A. J. Dennis

Rockwell International
Los Angeles Division
International Airport
Los Angeles, CA 90009
Attn: L. M. Lackman
D. Y. Konishi

Sikorsky Aircraft Division
United Aircraft Corporation
Stratford, CT 06602
Attn: Library

Southern Methodist University
Dallas, TX 75275
Attn: R. M. Jones

Southwest Research Institute
8500 Culebra Road
San Antonio, TX 78284
Attn: P. H. Francis

Space & Missile Systems Organization
Air Force Unit Post Office
Los Angeles, CA 90045
Attn: Technical Data Center

Structural Composites Industries, Inc.
6344 N. Irwindale Avenue
Azusa, CA 91702
Attn: R. Gordon

Texas A&M
Mechanics & Materials Research Center
College Station, TX 77843
Attn: R. A. Schapery

TRW, Inc.
23555 Euclid Avenue
Cleveland, OH 44117
Attn: W. E. Winters

Union Carbide Corporation
P. O. Box 6116
Cleveland, OH 44101
Attn: J. C. Bowman

United Technologies Research Center
East Hartford, CT 06108
Attn: R. C. Novak

University of Dayton Research Institute
Dayton, OH 45409
Attn: R. W. Kim

University of Delaware
Mechanical & Aerospace Engineering
Newark, DE 19711
Attn: B. R. Pipes

University of Illinois
Department of Theoretical & Applied Mechanics
Urbana, IL 61801
Attn: S. S. Wang

University of Oklahoma
School of Aerospace Mechanical & Nuclear Engineering
Norman, OK 73069
Attn: C. W. Bert

University of Wyoming
College of Engineering
University Station Box 3295
Laramie, WY 82071
Attn: D. F. Adams

U. S. Army Materials & Mechanics Research Center
Watertown Arsenal
Watertown, MA 02172
Attn: E. M. Lenoe
D. W. Oplinger

V.P. I. and S. U.
Dept. of Eng. Mech.
Blacksburg, VA 24061
Attn: R. H. Heller
H. J. Brinson
C. T. Herakovich